A&A 526, A119 (2011)
DOI: 10.1051/0004-6361/201015705

Astronomy & Astrophysics

Spectral properties of type Ia supernovae up to $z \sim 0.3$[⋆,⋆⋆]

J. Nordin[1,2], L. Östman[1,2,3], A. Goobar[1,2], R. Amanullah[1,2], R. C. Nichol[4], M. Smith[4,5], J. Sollerman[2,6,7], B. A. Bassett[5,8,9], J. Frieman[10,11], P. M. Garnavich[12,13], G. Leloudas[6], M. Sako[14], and D. P. Schneider[15]

[1] Department of Physics, Stockholm University, 10691 Stockholm, Sweden
e-mail: nordin@physto.se
[2] Oskar Klein Centre for Cosmo Particle Physics, AlbaNova, 10691 Stockholm, Sweden
[3] Institut de Física d'Altes Energies, 08193 Bellaterra, Barcelona, Spain
[4] Institute of Cosmology and Gravitation, Portsmouth PO13FX, UK
[5] Department of Mathematics and Applied Mathematics, University of Cape Town, Cape Town, South Africa
[6] Dark Cosmology Centre, Niels Bohr Institute, University of Copenhagen, 2100 Copenhagen, Denmark
[7] Astronomy Department, Stockholm University, AlbaNova University Center, 10691 Stockholm, Sweden
[8] South African Astronomical Observatory, Cape Town, South Africa
[9] African Institute for Mathematical Sciences, Muizenberg, Cape Town, South Africa
[10] Center for Particle Astrophysics, Fermi National Accelerator Laboratory, Batavia, Illinois 60510, USA
[11] Kavli Institute for Cosmological Physics, University of Chicago, Chicago, Illinois 60637, USA
[12] Harvard-Smithsonian Center for Astrophysics, 60 Garden Street, Cambridge, MA 02138, USA
[13] Department of Physics, 225 Nieuwland Science Hall, University of Notre Dame, Notre Dame, IN 46556, USA
[14] Department of Physics and Astronomy, University of Pennsylvania, Philadelphia, PA 19104, USA
[15] Department of Astronomy and Astrophysics, Pennsylvania State University, University Park, PA 16802 USA

Received 7 September 2010 / Accepted 18 November 2010

ABSTRACT

Aims. Spectroscopic observations of type Ia supernovae obtained at the New Technology Telescope (NTT) and the Nordic Optical Telescope (NOT), in conjunction with the SDSS-II Supernova Survey, are analysed. We use spectral indicators measured up to a month after the lightcurve peak luminosity to characterise the supernova properties, and examine these for potential correlations with host galaxy type, lightcurve shape, colour excess, and redshift.
Methods. Our analysis is based on 89 type Ia supernovae at a redshift interval $z = 0.05-0.3$, for which multiband SDSS photometry is available. A lower-z spectroscopy reference sample was used for comparisons over cosmic time. We present measurements of time series of pseudo equivalent widths and line velocities of the main spectral features in type Ia supernovae.
Results. Supernovae with shallower features are found predominantly among the intrinsically brighter slow declining supernovae. We detect the strongest correlation between lightcurve stretch and the Si II λ4000 absorption feature, which also correlates with the estimated mass and star formation rate of the host galaxy. We also report a tentative correlation between colour excess and spectral properties. If confirmed, this would suggest that moderate reddening of type Ia supernovae is dominated by effects in the explosion or its immediate environment, as opposed to extinction by interstellar dust.

Key words. methods: data analysis – techniques: spectroscopic – supernovae: general – cosmology: observations – line: profiles

1. Introduction

Cosmological distance measurements based on type Ia supernovae (SNe Ia) led to the discovery of the accelerated expansion of the Universe about a decade ago (Riess et al. 1998; Perlmutter et al. 1999), which requires that "dark energy" exist. This mysterious, hypothetical energy is one of the biggest puzzles in contemporary cosmology and fundamental physics.

With the ever increasing statistical precision on the density and equation-of-state parameter of dark energy, we are now reaching a point where systematic uncertainties are the limiting factors (Astier et al. 2006; Wood-Vasey et al. 2007; Kowalski et al. 2008; Hicken et al. 2009; Amanullah et al. 2010). This is emphasised in the first-year SDSS-II cosmology results (Kessler et al. 2009a; Sollerman et al. 2009; Lampeitl et al. 2010a). Two of the major (known) sources of systematic uncertainties when using SNe Ia to measure cosmological distances are the corrections for the colour-brightness relation and a possible drift with redshift of the SN brightness (e.g. Nordin et al. 2008). These shortcomings are related to our lack of any detailed understanding of the underlying physics preceding and during the explosion, including the progenitor system and both the circumstellar and interstellar environments.

Optical spectroscopy provides an excellent testbed for understanding SNe Ia: differences in explosion properties will likely modify spectral features. Although detailed 3D modelling may be needed to extract physical information (or parameters) from

⋆ Based on observations collected at the European Organisation for Astronomical Research in the Southern Hemisphere, Chile, in the ESO programmes 077.A-0437, 078.A-0325, 079.A-0715 and 080.A-0024. Also based on observations with the Nordic Optical Telescope acquired in the programmes with proposal numbers 34-004, 35-023 and 36-010.
⋆⋆ Appendices are only available in electronic form at http://www.aanda.org

observations, empirical techniques could provide important hints for future modelling. For example, comparisons between spectral properties for SNe with different host-galaxy type, lightcurve parameters and redshifts may be used to infer trends that affect their use as distance indicators.

There are indications of a population drift with redshift (Sullivan et al. 2006), which could be detectable as spectral evolution if the average (composite) spectra in different redshift bins are compared. Redshift dependencies in composite spectra have also been suggested by Foley et al. (2008) and Sullivan et al. (2009). While the metal content of the Universe increases with time, it is unclear to what degree increased metallicity actually propagates through the progenitor and explosion mechanisms to the outer ejecta of the supernova. If the element distribution of the ejecta is affected, this will likely change the observed spectrum (Lentz et al. 2000; Sauer et al. 2008).

An important question is whether the available low-z SN data sets correctly sample the demographics of SNe Ia at cosmological distances, or if there are subtypes of SNe not (yet) observed in the smaller local samples, but present at higher redshifts. Either case could yield an evolution of the average spectrum. Our data set at intermediate redshifts provides a useful sample to close the "gap" in studies currently available in the literature. We also study individual spectra and are thus potentially able to disentangle shifting population demographics from new subtypes.

It is also important to explore if there is any relation between SN Ia spectral features and broad-band colours. The colour-brightness relation of SNe Ia does not seem to match the Milky-Way dust extinction law (Riess et al. 1996; Tripp 1998; Krisciunas et al. 2000; Altavilla et al. 2004; Reindl et al. 2005; Astier et al. 2006; Guy et al. 2007; Nobili & Goobar 2008). The explanation may be connected to e.g., interactions in the circumstellar environment (Goobar 2008) or intrinsic SN properties, in which case a correlation of properties of spectral features and broad-band colours could be expected. Thus, comparisons of spectra of SNe with different colours may help in the understanding of the intrinsic colour dispersion in SNe Ia and allow us to disentangle the various components entering the colour-brightness relation and its possible evolution with redshift, critical for precision cosmology.

Relations between lightcurve parameters and host galaxy properties have been presented recently in Kelly et al. (2010); Sullivan et al. (2010) and Lampeitl et al. (2010b). These empirical findings call for further scrutiny; one way to do so is through comparisons with properties of SN Ia spectra.

Although a number of spectral feature comparisons of SN spectra have been performed in recent years (e.g. Hook et al. 2005; Benetti et al. 2005; Branch et al. 2006; Blondin et al. 2006; Garavini et al. 2007a; Foley et al. 2008; Bronder et al. 2008; Ellis et al. 2008; Sullivan et al. 2009; Wang et al. 2009; Bailey et al. 2009), we are still far from a complete understanding of the observed variation of SN Ia spectra. Detailed spectral studies are needed in order to limit the possible differences between low and high redshift objects, a basic requirement for the use of SNe Ia as distance indicators, and could potentially be used to further sharpen the standarizable candle through secondary brightness indicators.

During 2006−2007, 169 spectra of SNe Ia were obtained at the New Technology Telescope (NTT) and the Nordic Optical Telescope (NOT) in a program designed for spectral identification of objects detected by the Sloan Digital Sky Survey II (SDSS-II) Supernova Survey (Gunn et al. 1998; York et al. 2000; Frieman et al. 2008). The SDSS-II Survey operated as a three-year survey (2005−2007), aiming at finding a large number of intermediate-redshift SNe Ia, to be used to estimate cosmological parameters. The search algorithm and the procedure for the spectroscopic observations have been described in Sako et al. (2008). The first-year photometry and spectroscopy have been presented in Holtzman et al. (2008) and Zheng et al. (2008), respectively.

The NTT/NOT SDSS spectra provide a key opportunity to study SN properties. First, the SN population is drawn from an interesting redshift range, where evolution could be expected, yet the SNe are close enough to yield a reasonably high S/N. Secondly, this data set is large enough to allow statistical tests. This data set is described in detail in Östman et al. (2010).

We present quantitative measurements of 89 SN Ia spectra from the NTT/NOT samples with good lightcurves and low to moderate host-galaxy contamination and compare these with samples of nearby SNe Ia. We focus on potential evidence of evolution, but also study correlations with lightcurve properties, such as stretch and colour, as well as host galaxy properties like stellar mass and star formation rate.

The two main sources of systematic uncertainties in spectral studies of SNe Ia are noise degradation and host galaxy contamination. These effects complicate the search for potential spectral evolution, and would cause systematic errors since they will affect nearby and distant SNe differently. An unknown systematic bias could be misinterpreted as a sign of evolution, or even obscure a real effect.

The analysis of spectral indicators presented here consists of several steps:

- We first compare NTT/NOT spectra with nearby data (Sect. 4). Deviating SDSS SNe, possible signs of *evolution*, are collected into a *deficit* subsample (named so since measurements are smaller than average).
- We then change focus and combine all data in order to search for correlations with global SN parameters (Sect. 5). We use LC parameters (SALT and MLCS2k2) and host galaxy properties and search for the epoch ranges with the most significant correlations.
- We finally try to understand the *origin* of both the deficit subsample and the major correlations with global parameters (Sect. 6). This is done through (i) studying the spectral region around 4000−4500 Å (rest frame); (ii) a comparison of *deficit* SNe with normal SNe and (iii) a short discussion of host galaxy correlations.

Through each step of this analysis, focus has been put on minimising/mapping any sort of systematic error and/or observer bias. The observations, data reduction and host galaxy subtraction methods of the NTT/NOT spectra are presented in Östman et al. (2010), while comparisons of indicator measurements will be presented here. Extensive Monte Carlo simulations were run in order to estimate errors caused by host galaxy subtraction or varying noise levels.

The full organisation of this paper is as follows: in Sect. 2 we introduce spectral indicators and in Sect. 3 we present the data sets used. In Sect. 4 the indicator measurements, as a function of spectral epoch, are displayed for both the NTT/NOT and the reference SNe. Section 5 contains studies of the correlations between spectral indicators and lightcurve parameters as well as with host galaxy properties. Section 6 contains a discussion (focused on evolution and the Si II λ4000 feature) and finally conclusions are given in Sect. 7. We present further details of our Monte Carlo tests in Appendices A and B. All SNe included in this study can be found listed in Appendix C.

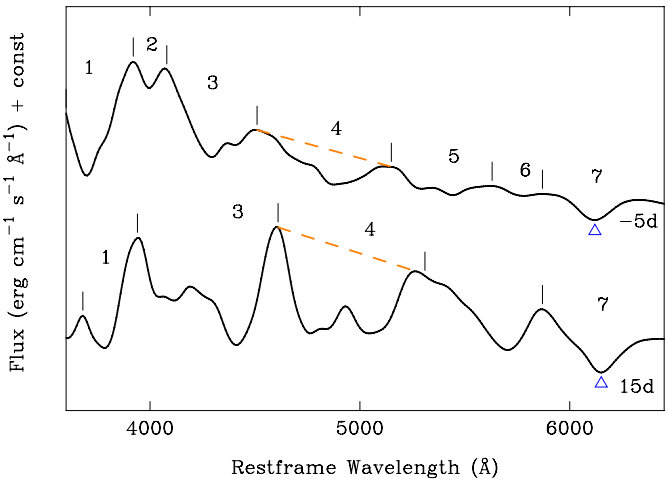

Fig. 1. The feature regions used for the measurements of spectral indicators are shown for two template spectra at day −5 and 15 relative to lightcurve peak (templates from Hsiao et al. 2007). The *pseudo* continuum (dashed orange) and line minimum (marked with blue triangle) are shown for two features (feature 4 and 7, respectively).

2. Spectral indicators

Elements in the SN ejecta will absorb photons originally emitted by radioactive material in the inner layers, thus causing the typical pattern of "features" visible in SN Ia spectra. In this analysis of spectral features we concentrate on seven regions corresponding to these studied by Folatelli (2004) and Garavini et al. (2007a). In Fig. 1, the features are displayed for a typical spectrum at two different ages.

Each feature is labelled after the ion that normally dominates the absorption in this region (see Table 1), but since most absorption lines are blends of several lines and should not be directly identified with physical properties, these regions will simply be identified as features 1 to 7.

With the term "spectral indicator" we refer to a measurement of a spectral feature of a SN Ia spectrum. Spectral indicators are always measured on rest-frame spectra, and all spectra presented here have been de-redshifted. In this paper we will discuss two indicators, pseudo Equivalent Widths (pEWs) and velocities. Feature 5, shaped like a "w", has two minima; we use the redder of these as velocity indicator.

2.1. Pseudo equivalent widths

For astrophysical objects with a well-defined continuum, the equivalent width of an absorption feature can be measured easily. If, furthermore, the density structure is known and the absorption is caused by a single ion, this information can be used to deduce elemental abundances. For SNe Ia, the spectra are dominated by wide absorption features caused by mixed multiple absorption lines. The continuum can thus not be read directly from the observed data, and the physical interpretation of equivalent widths becomes non-trivial. Nevertheless, we can measure equivalent widths if an unambiguous (pseudo) continuum can be *defined*. We do this following Folatelli (2004) and Garavini et al. (2007a). A lower and upper *limit* is found at the peak-flux wavelength within lower and upper wavelength *regions*. These regions, for the features used here, are given in Table 1. The pseudo-continuum is defined as the straight line between the flux of these lower and upper limits, with the choice of peaks

Table 1. Feature boundaries (pEW).

Feature	Dominating line	Lower region (centre Å)	Upper region (centre Å)
f1	Ca II H&K	3450–3800	3800–4100
f2	Si II λ4000	3800–3950	4000–4200
f3	Mg II λ4300	3850–4250	4300–4700
f4	Fe II λ4800	4300–4700	4950–5600
f5	S II W	5050–5300	5500–5750
f6	Si II λ5800	5400–5700	5800–6000
f7	Si II λ6150	5800–6100	6200–6600

optimised so that the pseudo continuum is maximised while not intersecting the spectrum.

With this pseudo-continuum a (pseudo) Equivalent Width (pEW) can be calculated (using the standard equivalent width formula):

$$\mathrm{pEW} = \sum_{i=1}^{N} \left(1 - \frac{f(\lambda_i)}{f_c(\lambda_i)}\right) \Delta\lambda_i, \quad (1)$$

where f is the observed flux and f_c is the pseudo-continuum. The sum is taken over all wavelength bins contained between the lower and upper limit.

The pEW definition has the advantage of not having to fit any function to the data (most features are clearly non-Gaussian) as well as being insensitive to multiplicative differences between spectra (assuming the multiplied factor does not change drastically over the range of the feature). However, pEWs are not insensitive to additive flux differences.

As for equivalent widths, the *statistical* error is given by

$$\sigma^2_{\mathrm{pEW}} = \sum_{i=1}^{N} \left(\frac{\sigma_f^2(\lambda_i)}{f_c^2(\lambda_i)} + \frac{f^2(\lambda_i)}{f_c^4(\lambda_i)}\sigma^2_{f_c}(\lambda_i)\right) \Delta\lambda_i^2. \quad (2)$$

It consists of two parts, the first is obtained from the error spectrum, σ_f, while the second propagates the uncertainty from the choice of pseudo-continuum, σ_{f_c}.

To avoid subjectivity in the pEW measurements, all steps were automated, e.g. the level of filtering was determined through lookup tables (see below and Appendix B) and boundaries for the pEWs are determined using computer algorithms. The automated code was validated by measuring the pEWs on the same data as Garavini et al. (2007a). The same indicator trends were obtained when using the same input spectra[1].

In addition to the statistical error, there are several sources of systematic uncertainties. Host-galaxy contamination can both change the shape of the feature and induce an additive flux change. Differential slit loss effects, which although being multiplicative can have large effects on the host-galaxy subtraction process, are included in contamination errors. These systematic pEW uncertainties are discussed below.

Noise-filtering uncertainties Filtering or smoothing is necessary in order to identify the end points of spectral features. However, the optimal filter parameters will change with Signal-to-Noise (S/N) ratio; noisy data need stronger smoothening to reduce the impact of random fluctuations in choosing the feature endpoints, while the same filter strength will dilute information

[1] As a further check on these algorithms the automatic measurements were manually revised and the outcome compared with our basic results. No major deviations were seen.

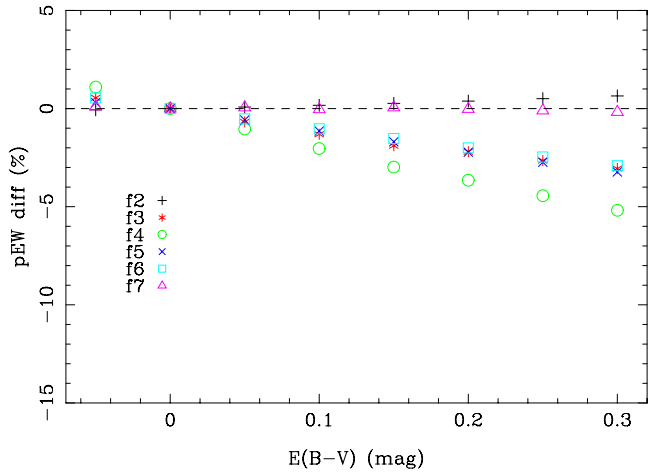

Fig. 2. Percent change in pEW for features 2 to 7 as a function of $E(B-V)$. The measurements are based on the Hsiao et al. (2007) SN template at peak brightness and assuming Cardelli et al. (1989) type dust with $R_V = 1.7$.

in high S/N data. Over or under filtering can introduce a measurement bias. This is a particular concern when making redshift comparisons, since distant SNe have (in general) lower S/N than nearby SNe.

Extensive Monte Carlo (MC) simulations were carried out to make an optimal choice between filtering methods and their parameters. The simulations are described in detail in Appendix B. We conclude that a standard boxcar smoothing performs well, provided that the boxcar width is modified depending on the noise level of the spectrum and what feature is being studied. The simulations were used to find the optimal boxcar width for each S/N. For each feature and S/N level we also obtain an uncertainty from the simulations which is added in quadrature to the systematic pEW error.

Host-galaxy contamination uncertainties. The host galaxy contamination is the single largest source of systematic errors for pEW studies. Unsubtracted host light can both cause an error through a flux offset and, if the underlying galaxy is changing with wavelength, through shifting pEW feature boundaries. Monte Carlo simulations were performed to estimate the uncertainties due to the host-galaxy subtraction. When host galaxy contamination could be estimated using photometry, both the error and a possible bias is retrieved as a function of contamination (this is the case for all NTT/NOT spectra as will be discussed below). For spectra where no host-galaxy is subtracted (reference spectra and low contamination SDSS spectra) we add the uncertainty expected for an uncorrected 10% galaxy contamination. See Appendix A for a more detailed description of these simulations.

Reddening. Pseudo-equivalent widths are also affected by uncorrected reddening by host-galaxy dust. In Fig. 2 we show how pEWs, as measured on a template spectrum, change as dust-like extinction is applied to the template. All features gradually *decrease* with colour excess, $E(B-V)$. Changes are smaller than 10% for $E(B-V) \leq 0.3$ mag. As expected, wider features change more with extinction than narrower ones.

Table 2. Feature minima wavelengths.

Feature	Dominating line ($\sim\lambda$ observed)	Rest wavelength (Å)
f1	Ca II H&K	3945.12
f2	Si II (λ4000)	4129.73
f3	Mg II (λ4300)	4481.20
f4	Fe II (λ4800)	5083.42
f5	S II W	5536.24
f6	Si II (λ5800)	6007.70
f7	Si II (λ6150)	6355.21

2.2. Line velocities

The position of absorption and emission features can also be used to probe SN properties. We study the wavelength minima of the features defined above. As reference minima we use the *rest* wavelength of the ion that each feature was named after, these are given in Table 2 (3rd column).

These are converted into velocities through the relativistic Doppler formula,

$$v_{\rm abs} = c\,\frac{(\lambda_m/\lambda_0)^2 - 1}{(\lambda_m/\lambda_0)^2 + 1}, \tag{3}$$

where λ_0 is the laboratory wavelength of the ions creating the feature and λ_m is the measured wavelength in the rest-frame of the host galaxy (SNe without host galaxy redshifts are thus excluded from velocity studies).

As for pEWs, it is difficult to give a direct physical interpretation of line velocities for SNe Ia since most spectral features consist of blends of ions. Also, different ions dominate features at different epochs and thus shift the minimum position. Nonetheless we use the same reference wavelength, with the consequence that measurements are not guaranteed to be the velocity of an ion, but are rather a general measurement that can be compared between different SNe. In practice we only study each feature during epochs where no drastic changes happen to the minima shape. Some of the features lack clear minima, like feature 4, and are thus harder to evaluate. Si II λ6150 (f7), typical of SNe Ia, most often yield unambiguous measurements and is thus usually the best estimate of the "true" expansion velocity.

All spectra are binned using bin widths constant in velocity, $c\Delta\lambda/\lambda = 2000$ km s^{-1}. Binned error spectra were calculated through weighted error averages in each bin.

The flux minima for the different features were obtained in the binned spectra, i.e. without interpolation to a finer wavelength grid and without fitting a general shape to the region. Although a sub-bin fitting procedure would, in principle, give a finer determination of the minimum, this is not viable with the noise level in our sample.

Velocity error estimates. Velocity measurements are less sensitive to most major systematic uncertainties, but noisy or heavily contaminated spectra can still have substantial uncertainties. These were studied using similar Monte Carlo simulations as for pEWs, see Appendix A and B. For noisy or contaminated data, the dispersion is non-negligible, but leads to no major bias, provided host-galaxy subtractions are performed on host contaminated spectra.

Systematic uncertainties obtained from the simulations are added to each velocity measurement depending on the S/N and the estimated contamination. These are added in quadrature with a 200 km s^{-1} peculiar velocity error.

3. Data sets

Our sample consists of SNe Ia observed with the NTT and the NOT as a part of the SDSS-II Supernova Survey (Östman et al. 2010). The set consists of 169 SN Ia spectra of 141 different objects. SDSS SNe are labeled after their SDSS Supernova ID number, see Östman et al. (2010) for the respective IAU names.

Observations made at the NTT were performed using the ESO Multi-Mode Instrument (EMMI) and have a wavelength coverage from 3800 to 9200 Å, a wavelength dispersion of 1.74 Å per pixel, and a spatial resolution of 0.″166 per pixel before binning. A binning of 2 × 2 was used. The NOT spectra were obtained using the Andalucia Faint Object Spectrograph and Camera (ALFOSC) with grism 4. NOT spectra have a wavelength range from 3200 to 9100 Å, a wavelength dispersion of 3.0 Å per pixel, and a spatial resolution of 0.″19 per pixel. See Östman et al. (2010) for detailed information.

Lightcurve properties such as stretch, colour and maximum absolute magnitude, as well as the spectral epochs, were obtained with the SALT lightcurve fitter (Guy et al. 2005). The spectral *epoch* is defined with respect to the peak of the *B*-band lightcurve.

After applying lightcurve quality cuts, requiring photometric observations both prior and post maximum brightness, we are left with 127 spectra. Out of these, 116 spectra have both good host-galaxy subtraction and are of sufficient quality for spectral features to be identified. Finally, we apply a host-galaxy contamination cut of <60% in the *g*-band, motivated by Monte Carlo simulations, which leaves us with 89 spectra[2]. A list of all NTT/NOT spectra used in this analysis is given in Table C.2.

The SDSS NTT/NOT spectra are compared to a low-redshift reference SN sample which consists of three subsets, data from the Harvard-Smithsonian Center for Astrophysics (CfA), the Supernova Cosmology Project (SCP99) and the Online Supernova Spectrum Archive (SUSPECT). Since the NTT/NOT spectra cover the spectral epochs between −9 days and +20, we have only studied reference spectra up to epoch 30.

The CfA sample consists of 162 spectra of 19 SNe Ia from Matheson et al. (2008). The SCP99 data set contains 79 spectra of 16 SNe observed by the Supernova Cosmology Project in 1999 that were studied by Garavini et al. (2007a). The SUSPECT data set collects publicly available SN spectra[3], we use 421 spectra of 40 type Ia SNe. A list of all spectra in our reference sample is given in Table C.1. The table also contains the source of the lightcurve parameters as well as the original spectroscopic reference for SUSPECT spectra. These lightcurve parameters are lacking for some SNe and these objects are thus excluded from analysis where such information is required.

We present in Fig. 3 the distribution of epoch, redshift, SALT stretch and SALT colour for the NTT/NOT sample together with the reference sample used in this paper.

The NTT/NOT sample has significantly larger redshifts than the comparison sample, a median value of $\bar{z}_{\rm SDSS} = 0.17$ compared to $\bar{z}_{\rm ref} = 0.01$. The spectral epoch distribution is also somewhat different: the NTT/NOT spectra are more centred around the lightcurve peak, while the comparison sample includes earlier and later epochs. This is a natural effect arising from the differing magnitude limits of the SN searches. The distribution of SALT stretch is fairly constant between the samples with a Kolmogorov-Smirnov (KS) probability of 5%, thus showing that we can not reject the assumption that they belong to the same distribution. The median value for the NTT/NOT sample and the reference sample are 0.96 and 0.94, respectively. However, the SALT-*c* (colour) distributions are significantly different as can been see by a visual inspection, with a tail of red colour SN in the reference sample. This is not surprising since local SNe Ia can be detected even with a few magnitudes of extinction. The median value for the NTT/NOT sample and the reference sample are 0.05 and 0.10, respectively.

While the SALT lightcurve fit output is used to make the initial analysis, we have also obtained MLCS2k2 (Jha et al. 2007) lightcurve fits. MLCS output consist of a lightcurve shape-dependent parameter Δ and the *V*-band extinction, A_V. The A_V parameterisation assumes that any reddening not corrected for by the Δ parameter can be described by a Milky Way-like extinction law. These fits are used to validate results found using SALT and study lightcurve fit dependant effects. We use the MLCS lightcurve fits of all reference SNe contained in the Hicken et al. (2009) data set together with MLCS fits of the NTT/NOT SDSS SNe obtained using the SNANA fit package (Kessler et al. 2009b) and employing the same quality cuts and settings as in Kessler et al. (2009a). The only exception to this procedure was that we used $R_V = 1.7$, this change was made to comply with Hicken et al. (2009) but has very small effect on our analysis.

In Östman et al. (2010) three potential peculiar SNe Ia from the NTT/NOT data set are presented: two of SN1991T-type and one SN2002cx like. In this paper we can not confirm any additional "SN1991T", "SN1991bg" or "SN2002cx" SNe. Li et al. (2010) find, in their luminosity limited sample, that 77% of all type Ia SNe are normal, 18% SN1991T-like, 4% SN1991bg-like and 1% SN2002cx-like. While "SN1991bg" and "SN2002cx" either would have escaped detection entirely, due to their low luminosity, or have been singled out based on lightcurve properties, it is likely that a fraction of the SNe used here are really of the "SN1991T"-type. That these are not identified can be explained by two effects: (i) the S/N is often good enough to classify a SN as Ia, but not high enough for a strict subclassification (Östman et al. 2010) (ii) "SN1991T" like SNe are often mistaken for normal if no early spectra exist (an "age bias", Li et al. 2010). We will later, in Sect. 6, show that a fraction of ∼20% of the SDSS SNe have shallower features and would represent "SN1991T" like SNe at later epochs well.

The NTT/NOT spectra have well documented uncertainties (Östman et al. 2010). However, most of the spectra in the reference sample lack error estimates. For such cases, a constant flux error of 5% of the average spectral flux was used to compute the uncertainties in spectral indicators.

3.1. Host galaxy subtraction

A large fraction of the SDSS NTT/NOT SNe have significant host galaxy contamination which could affect spectral indicators. In particular, comparisons with virtually host-free spectra for local reference SNe could lead to systematic differences that may be confused with evolution with redshift. Great care was taken to remove the host galaxy light efficiently, given the data available, as well as understanding remaining errors.

A large fraction of the NTT/NOT SNe were not observed in paralactic angle, and are thus affected by differential slit losses. In Östman et al. (2010) we calculate slit loss for all spectra, as functions of estimated seeing conditions and centring wavelength. Because of the uncertainties associated, mainly regarding

[2] This limit is somewhat arbitrary: many subtractions of higher contaminated spectra succeed, but the risk of a subtraction significantly failing increases above 60% host contamination. See Appendix A.

[3] http://bruford.nhn.ou.edu/suspect/

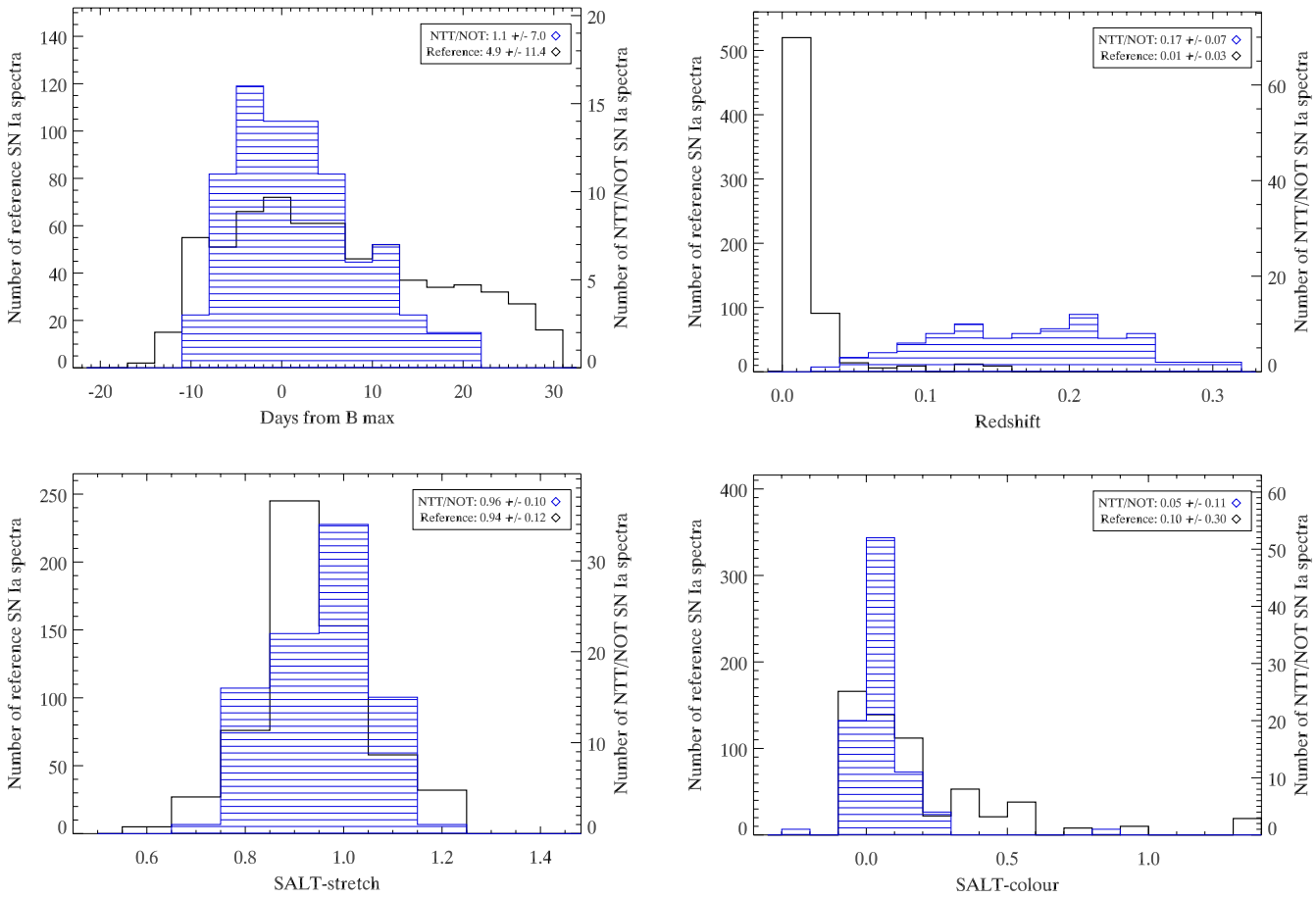

Fig. 3. Distribution of epoch, redshift, SALT stretch factor and SALT colour for the SN spectra used in our study. The epoch is defined here as the number of days in rest frame from B band maximum brightness. The white histogram is for the reference sample while the striped histogram is for the NTT/NOT spectra used here. Legends show mean and Gaussian 1σ levels for the subsets.

centring, we choose not to apply calculated slit losses directly to the spectra, but rather to incorporate corrections into the host subtraction pipeline, where we also account for reddening. Considering the typical centring wavelength (6500 Å) and the limited wavelength range studied (4000−6500 Å), slit loss and reddening exhibit similar differential attenuation and can be fitted together.

A detailed description of the host galaxy subtraction can be found in Östman et al. (2010). In brief, the galaxy SED which is subtracted is estimated by minimising the difference between the observed spectrum and a combination of a SN template and a set of galaxy eigenspectra. To the SN template, a second degree polynomial is multiplied to account for reddening (e.g. due to host galaxy dust extinction) and differential slit loss effects. The minimisation can be described with the formula

$$f_{\rm fit}(\lambda) = a_0 s(\lambda) \cdot f_{\rm SN}(\lambda) + \sum_{i=1}^{3} a_i g_i(\lambda), \quad (4)$$

where $f_{\rm SN}$ is the SN template, g_i the galaxy eigenspectra, s the second degree polynomial and a_i weights which are fitted in the subtraction. The SN templates in the fit were the Hsiao templates (Hsiao et al. 2007) within epochs ±5 days from the SN spectral epoch as obtained from the lightcurves. Models of the peculiar SNe 1991bg and 1991T (Nugent et al. 2002) within the same epoch interval were also included in the fit, but no new clear cases of these subtypes were found. Three galaxy eigenspectra from SDSS (Yip et al. 2004) were used for the galaxy SED in the fit. The second degree polynomial $s(\lambda)$ was locked to have $s \equiv 1$ at $\lambda = 6600$ Å and $s < 1$ for all other wavelengths (thus only having one degree of freedom). The wavelength of the s function peak is chosen to match the wavelength where most spectra were centred on the slit. It should be noted that the slit loss function is asymmetric around the centring wavelength, but the fit during subtraction is only made between 4000 and 6000 Å and thus the behaviour of s at longer wavelengths will not affect the fit. The polynomial is only multiplied with the SN SED, and not with the galaxy. This was done since galaxies, not being point sources, are significantly less affected by slit loss.

Several modified versions of this host subtraction were tried: other sets of eigencomponent spectra, more eigencomponent spectra, free polynomial (instead of restricted) and slit loss applied to the host galaxy. For individual spectra one of these alternative methods might achieve better fits, but globally they were all either less stable or as good but with significantly more parameters to fit.

Figure 4 shows subtraction samples of SNe with contamination ranging from very high (77%) to very low but including reddening/slit loss. For moderate contamination, 10 to 60% galaxy light in the g-band, the multiplicative host-galaxy subtraction works well. *Within these limits the best fit galaxy SED is subtracted from the observed spectrum before any measurements are done.* An error associated with host contamination uncertainties was calculated for each indicator measurement. In Fig. 5 we show examples of how host subtraction affects pEW measurements. For spectra with very low contamination, no subtraction is done and the error estimated for 10% unsubtracted

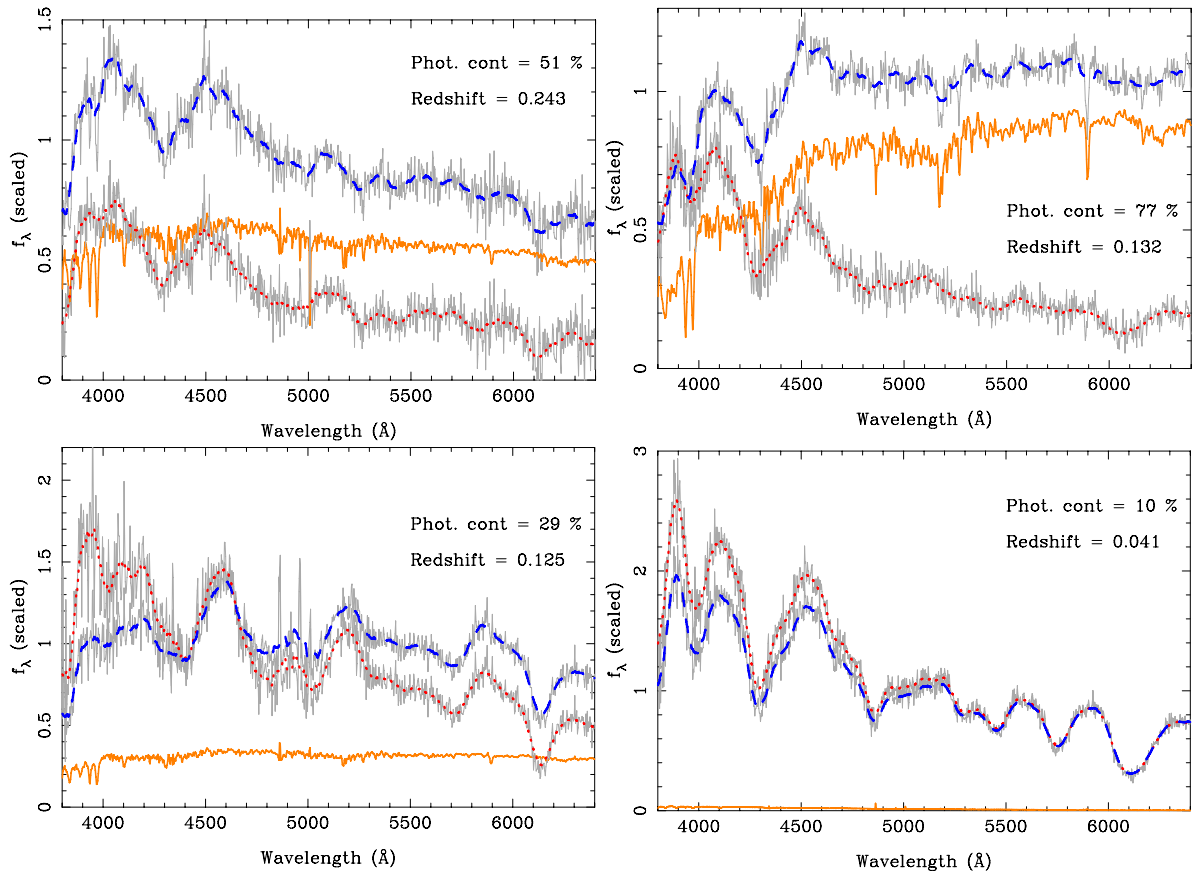

Fig. 4. Display of sample host galaxy subtractions of SDSS SN16637, 12907, 17886 and 13894 (clockwise *from top left*, restframe epochs −1, 0, −4 and 9). All flux values (y-axis) have been scaled. Wavelength (x-axis) is rest-frame wavelength. The grey line shows the unsmoothed original spectrum, while the dashed blue line shows the smoothed version. Dotted red line show final subtracted *slit loss/reddening corrected* spectrum and orange solid line show best fit galaxy. Note that because of the slit loss/reddening correction the galaxy and subtracted spectrum do not sum to the raw spectrum. The galaxy contamination estimated from photometry (g-band) and redshift have been written in each panel.

light added. Spectra with very high contamination are excluded from the analysis.

In Appendix A we describe simulations designed to estimate uncertainties and evolution detection limits. We have performed several tests in order to determine the stability of our results. These include comparisons with synthetic spectra and comparisons between different host galaxy subtraction methods.

The low-z reference sample spectra were *not* host subtracted. These are sufficiently local to allow subtraction of most host galaxy contamination during data reduction. Visually, they do not appear to contain significant host galaxy light.

4. Results: comparing the reference and NTT/NOT samples

After host subtraction all spectra are processed through the automated indicator measurement pipeline. The error bars of the measurements are symmetric geometric sums of the statistical uncertainty of the measured indicator and the noise-filtering and host-galaxy subtraction systematic errors.

All spectral epochs used are rest frame epochs and are thus corrected for time dilation.

4.1. The reference sample

The reference set measurements were combined into 1-σ contours to facilitate statistical comparisons. The contour is calculated for each day as the weighted mean and uncertainty of the indicator (pEW/velocity) for ±3 days. The broad epoch interval is used to make a smooth curve (stable with respect to outliers). As a justification for the definition of the band, the measurements underlying the band for pEW for feature 3 are shown in Fig. 6.

We confirm the displacement of the unusal SNe Ia compared to the overall trend, as shown in Fig. 7 for the reference sample. Peculiar SNe are not included in the reference sample, but it is in practise impossible to make a strict definition regarding which SNe should be considered as "normal". The number of observed spectra per SN also varies, thus giving artificially high weight to certain objects. *We thus do not expect the reference sample to completely match the NTT/NOT SNe detected in a rolling SN survey.* The fraction of SNe of different SN Ia subtypes are different, as well as the distribution of lightcurve color. We will return to possible consequences of this when discussing evolution in Sect. 6.

4.2. Pseudo-equivalent widths

Figure 8 shows the measured pEW values of features 2 to 7 for the NTT/NOT spectra as a function of epoch. These are compared to the corresponding 1σ contour for the normal SNe Ia in the reference sample. Features are only measured for epochs when they can be clearly defined.

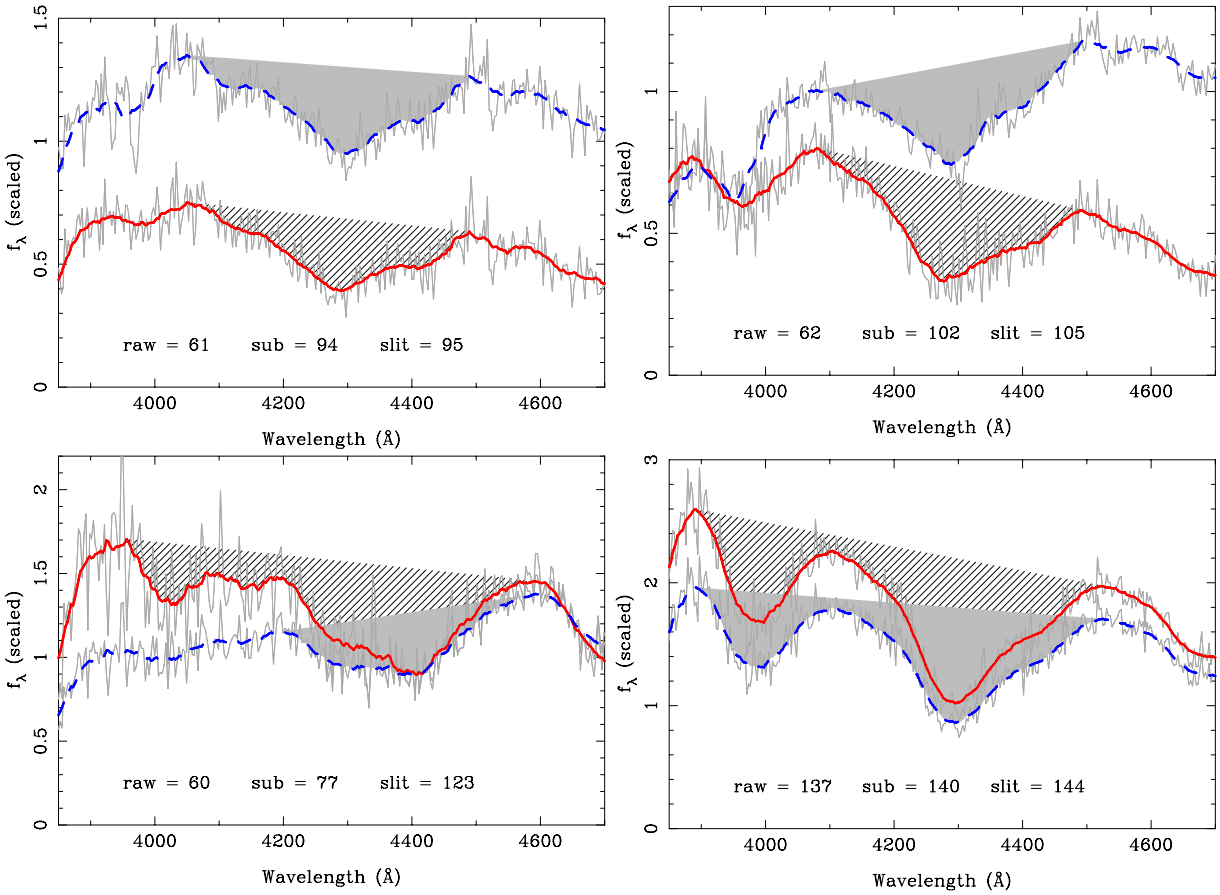

Fig. 5. Expanded view of the feature 3 region for the same spectra displayed in Fig. 4, showing the effects of host subtraction and slit loss/reddening correction on pEW. Wavelength (*x*-axis) is rest-frame wavelength. The blue dashed line is the raw spectrum, the red solid line the final subtracted and corrected spectrum. The marked regions show where pEW is calculated, the calculated pEWs (in Å) are written in panels for raw spectra ("raw"), subtracted spectra ("sub") as well as subtracted *and* corrected spectra ("slit"). These sample spectra show host subtraction change pEWs both through additive offsets and changed feature limits.

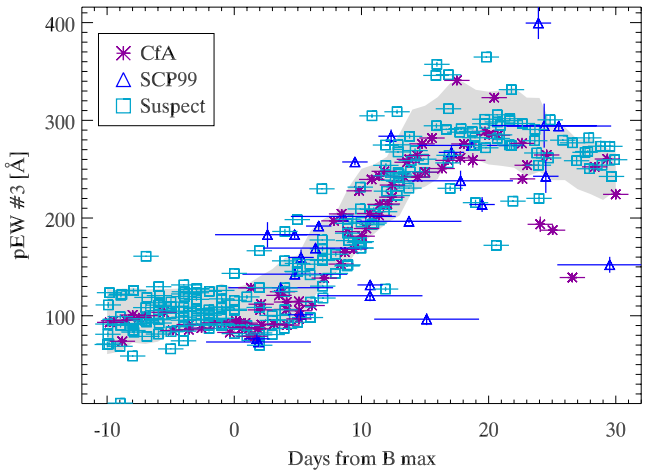

Fig. 6. pEW values for the reference data for f3 vs. epoch. The shaded region is the same one sigma contour as shown in the left panel of Fig. 8. The different symbols show the measurements that were used to construct the grey region, with different symbols denoting the different subsets of the reference sample.

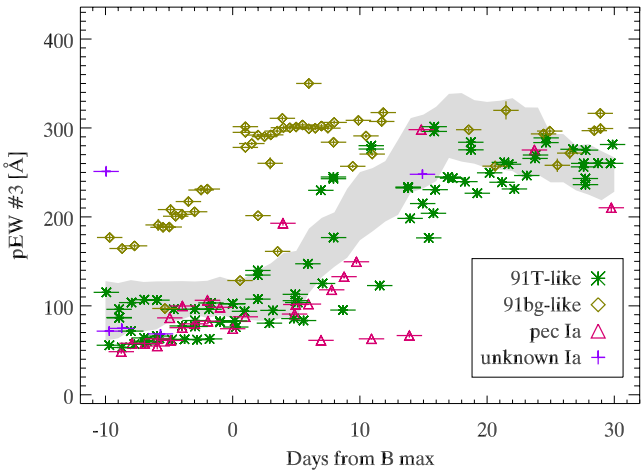

Fig. 7. Peculiar SNe compared with normal. The shaded region shows the one sigma contour constructed from the normal SNe Ia in the reference sample *and* the NTT/NOT spectra. The symbols show the measured pEWs for the SN 1991T-like, SN 1991bg-like and peculiar SNe Ia in the reference sample.

To be able to study the correlations of spectral indicators with different parameters we want to remove the epoch dependence. This is done by fitting a function describing the epoch evolution in pEW and then subtracting it from the

measurements[4]. This *epoch independent* quantity (ΔpEW) is shown in Fig. 9 for *all* SNe Ia NTT/NOT and reference spectra (including peculiar types) as a function of redshift for epochs around maximum brightness.

We now examine Figs. 8 and 9 for significant differences between distant and local SNe. The NTT/NOT measurements generally match the 1-σ contour of the reference sample within uncertainties. There are, however, some regions where the NTT/NOT pEW measurements appear, on average, *lower than the reference set average*. These differences appear most significent for pEW f2 and pEW f4, this is most easily seen in Fig. 9 (top left and mid left, shaded region).

In order to study the origin of these differences we collect all SNe with either *f2* or *f4 pEW measurements below those of normal SNe in the reference sample into a* pEW-deficit *sample* (thus ΔpEW-f2 < -8 Å OR ΔpEW-f4 < -25 Å). This subset is examined in detail in Sect. 6, where we for example discuss the effects of different lightcurve parameter distributions. The limits in pEW for the *deficit* sample are arbitrary; we do not expect them to precisely single out a physically distinct subset of SNe. It is rather to be seen as a starting point for a discussion of possible differences between local and distant SNe.

4.3. Comparing the two samples – line velocities

Figure 10 shows some of the more stable line velocities for the NTT/NOT sample together with the 1-σ contour for the normal SNe Ia in the reference sample. Only measurements of SNe with redshifts measured from galaxy lines are included, i.e. the subset of objects with redshifts measured from SN features are excluded here. No signs of sample differences are detected.

The epoch evolution of the velocity of f7 Si II λ6150 (with epoch) have been extensively studied (Benetti et al. 2005; Wang et al. 2009; Maeda et al. 2010). However, the NTT/NOT sample does not contain enough SNe with multiple spectra to measure velocity changes.

4.4. Summary: comparing the reference and NTT/NOT samples

The samples are generally consistent, possibly deviating in a subset of NTT/NOT SNe with pEW measurements below these for normal SNe Ia in the reference sample. These were collected in a *pEW-deficit* sample.

5. Results: correlations with SN parameters

The collected sample (both low- and high-z SNe) was used to search for correlations between spectral indicators and global properties of type Ia SNe. Since many of the features evolve with epoch, we study the epoch corrected pEW- and velocity-differences, ΔpEW and Δv, as introduced above. The correlation is calculated taking into account the estimated uncertainties of the indicators.

[4] Indicators that vary little or gradually with epoch are fitted with a linear function. Indicators that show sudden changes (like pEW f3) are fitted using a logistic function: $f(t) = A/(1 + e^{(t_{br}-t)/\tau}) + B$.

5.1. Correlation statistics

As the basic measure of correlation between measurements R_i, S_i, $(i = 1...n)$, we use Spearman's rank correlation coefficient,

$$r_S = \frac{\sum_i (R_i - \bar{R})(S_i - \bar{S})}{\sqrt{\sum_i (R_i - \bar{R})^2}\sqrt{\sum_i (S_i - \bar{S})^2}} \cdot \quad (5)$$

This is similar to the Pearson correlation coefficient, i.e., a non-parametric measure of correlation, but relies on ranked variables. This method is preferable for variables not following a Gaussian distribution. Spearman's rank correlation is also less sensitive to outliers. The output coefficient range from -1 to 1, with -1 being perfect negative correlation, 0 no correlation and 1 being perfect positive correlation. The significance of a correlation r from n elements can be estimated roughly using Student's t distribution of dimension $(n-2)$ and $t = r\sqrt{(n-2)/(1-r^2)}$ (Press et al. 1992). For example, rank correlation 0.6 corresponds to less than 1% chance of being random if $n \gtrsim 18$. In our analysis we mark any correlation $r > 0.6$ where $n \gtrsim 15$ for further study. More realistic confidence analysis should be done using permutation tests. This is done when using flexible ranges below, where we account for the fact that we probe a large number of correlations (and thus expect statistical fluctuations to cause some large $|r|$). We first present the basic correlation coefficients for spectra close to lightcurve peak.

5.2. Correlations with lightcurve parameters

Correlations around lightcurve peak. We have searched for correlations with SALT stretch and colour as well as absolute magnitude, M, for spectra within ±3 days from maximum brightness. The absolute magnitude is corrected for stretch and colour and calculated assuming a fiducial cosmology. Table 3 lists the calculated Spearman coefficients. The statistical significance in standard deviation from the null correlation hypothesis is shown in parenthesis. At least 50 measurements were used in each correlation estimate.

Some pseudo-equivalent widths around peak luminosity do show strong correlation with lightcurve parameters. These include f2 and f7 correlating with stretch and f4 showing a correlation with lightcurve colour. In Fig. 11 we show these strong correlations, together with the f6 correlation with stretch. For the latter, all SNe except the low S/N NTT/NOT objects show a strong correlation; this feature is too small to probe among noisy data. The correlation of the depth of this feature with lightcurve width has been reported earlier, see e.g. Hachinger et al. (2008).

Also noticeable is that most correlations have the same *direction* (sign): SNe with wide lightcurves (large stretch) have weaker pEW values and redder SNe (large colour) have in general larger equivalent widths. While these colour correlations are not strong they are consistent and *opposite* in direction to what would be expected from an application of pure Cardelli et al. (1989) type extinction (see Fig. 2).

Any correlation between spectral indicators and peak magnitudes *corrected for stretch and colour* would be of great interest, since this could be used to "sharpen" type Ia SNe as standard candles. Most spectral indicators correlate only weakly with absolute magnitude (after correction for stretch and colour). The most significant correlation is for pEW f4; this is, however, a weak correlation of only moderate significance ($\sim 3\sigma$).

We find that none of the velocities are strongly correlated with stretch, colour or absolute magnitude around peak brightness. The kinetic energy, as sampled by line velocities, thus appear to be independent from the optical luminosity.

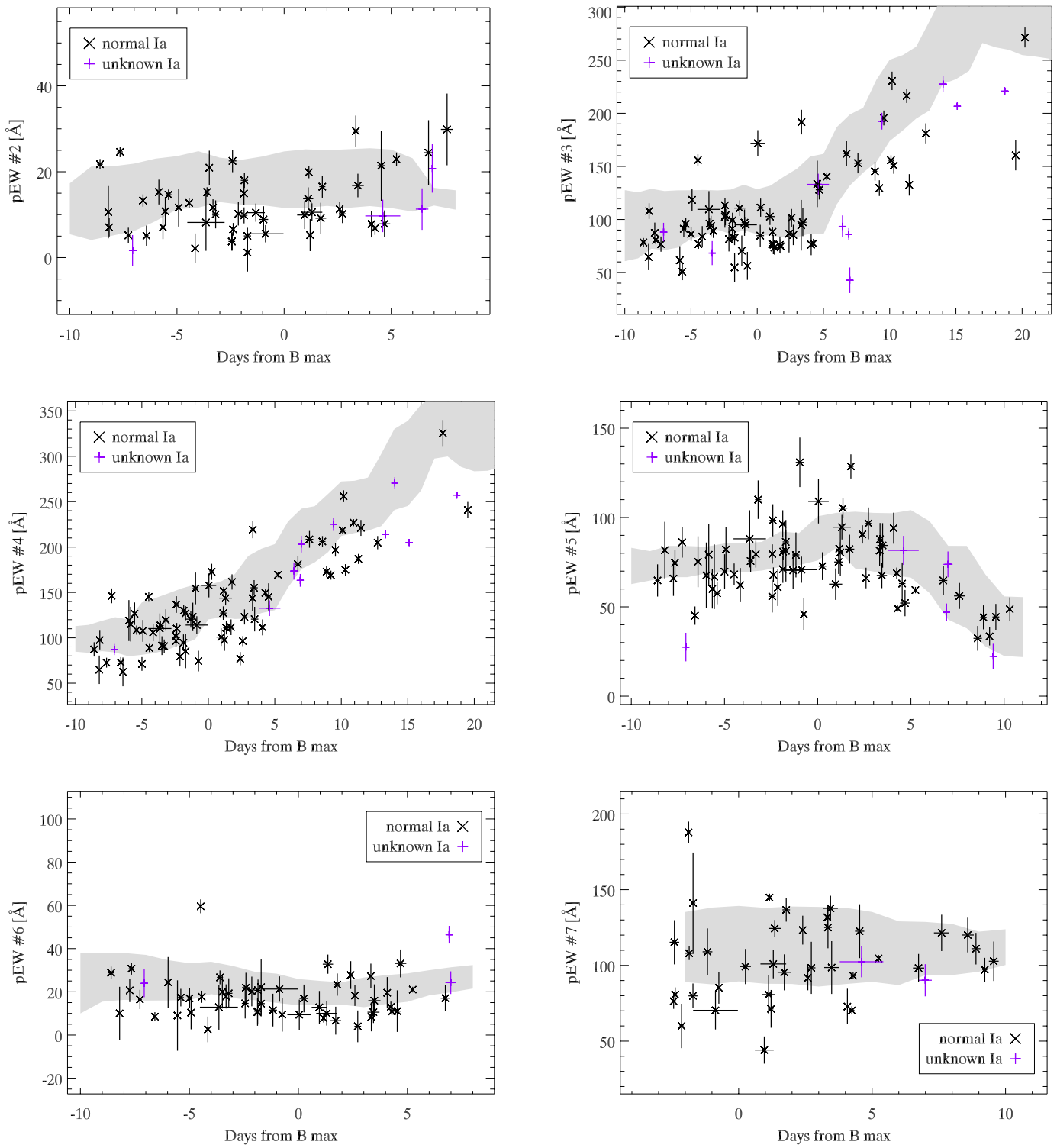

Fig. 8. Study of pseudo-equivalent widths for feature 2 to 7 vs. epoch. The shaded band shows the one sigma contour for the normal SNe Ia in the reference sample. The points show the measurements on the NTT/NOT spectra, where the error bars include both statistical and systematic errors. The different symbols show two categories: spectra identified as of the normal SNe Ia subtype by SNID (SuperNova IDentification; Blondin & Tonry 2007) or spectra identified as SNe Ia but of unknown subtype.

Flexible epoch ranges. There is no a priori reason to expect a fixed epoch range around lightcurve peak to be the epoch range where spectral indicators correlate best with lightcurve parameters. In Fig. 12 we present a sample of the bracketed epoch ranges where the most significant correlations were found through a blind search involving all indicators. Before analyzing the results we will describe the blind search in detail, as well the MC studies performed in order to determine how significant the search output is.

For a given set of epochs, an indicator measurement (e.g. pEW f2) and a global property (e.g. stretch), we loop through all epoch ranges (containing at least 15 measurements) and save any correlations with $|r_S| > 0.4$. A combination is thus defined by (spectral indicator, global property, min epoch, max epoch) e.g.

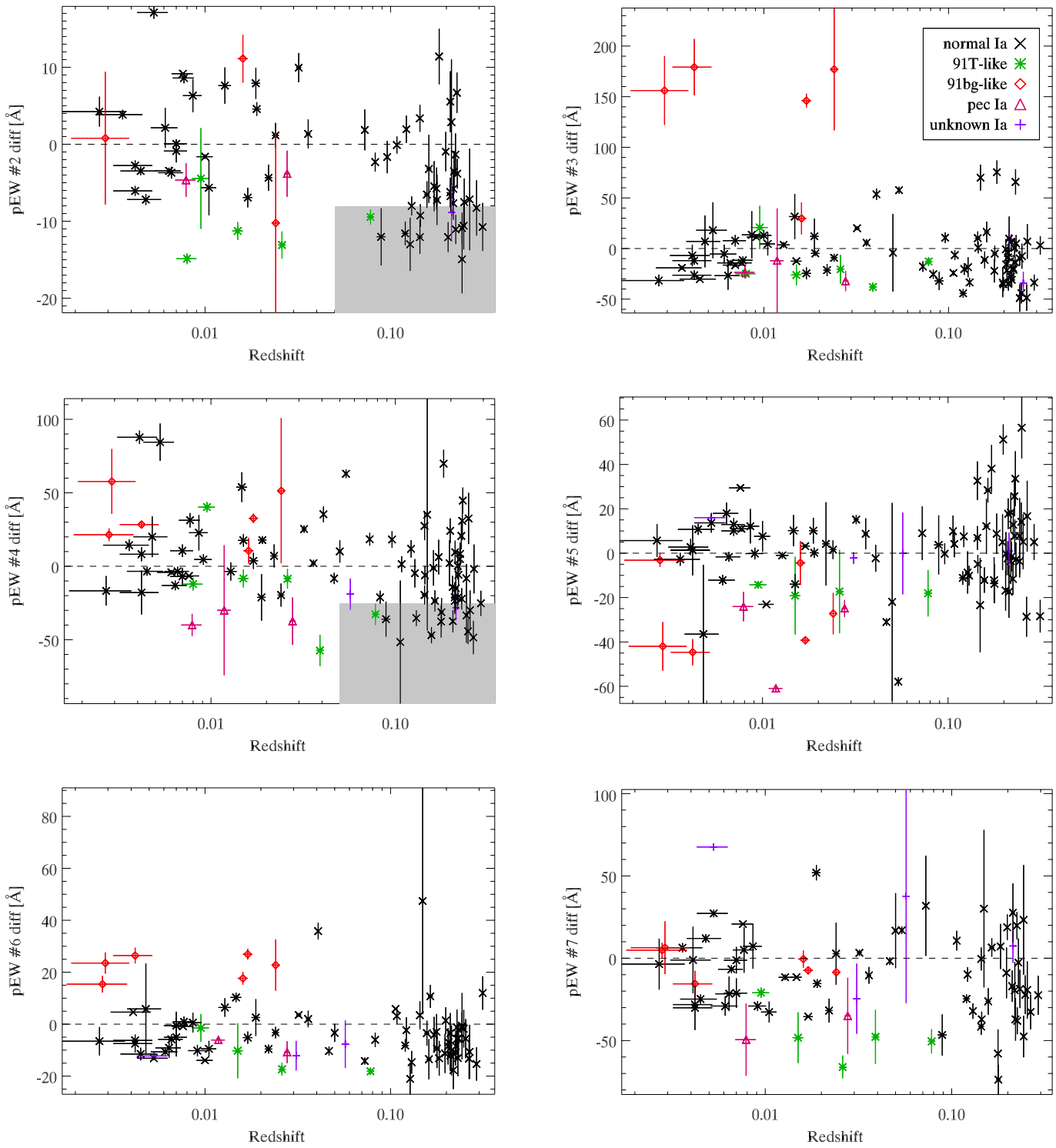

Fig. 9. Comparison of the pseudo-equivalent width measurements around lightcurve peak for features 2 to 7 vs. redshift. In all figures the average spectroscopic evolution *among non-peculiar low-z reference SNe* has been subtracted. It is thus the *pEW-difference* (compared to normal low-z SNe) that is plotted on the y-axis. SNe are divided according to subtype classification, with the colour scheme following the legend in the upper right plot. In *the two upper left panels* (f2 and f4) the shaded region show how the *pEW-deficit* sample is defined.

("pEW f2", "stretch", −8, 0). The number of such combinations, for each indicator, range from 500−1000 (if using all SNe and an indicator well defined at all epochs) to 50−100 (if using a subset of SNe and an indicator not existing at all epochs).

For any real correlation found we also expect "neighbouring" epoch ranges to be correlated. If, for example, the epoch range 0−8 yields a strong correlation we would also expect epoch ranges like 1−7 and 2−9 to show correlation. We thus rank correlations between indicators and global properties through the *number of epoch ranges with* $|r_S| > 0.4$. When we discuss a correlation in an epoch range, this is thus only one in a series of neighbouring correlating epoch ranges.

While this epoch bracketing is necessary in order to find the epoch ranges where indicators are sensitive to global parameters,

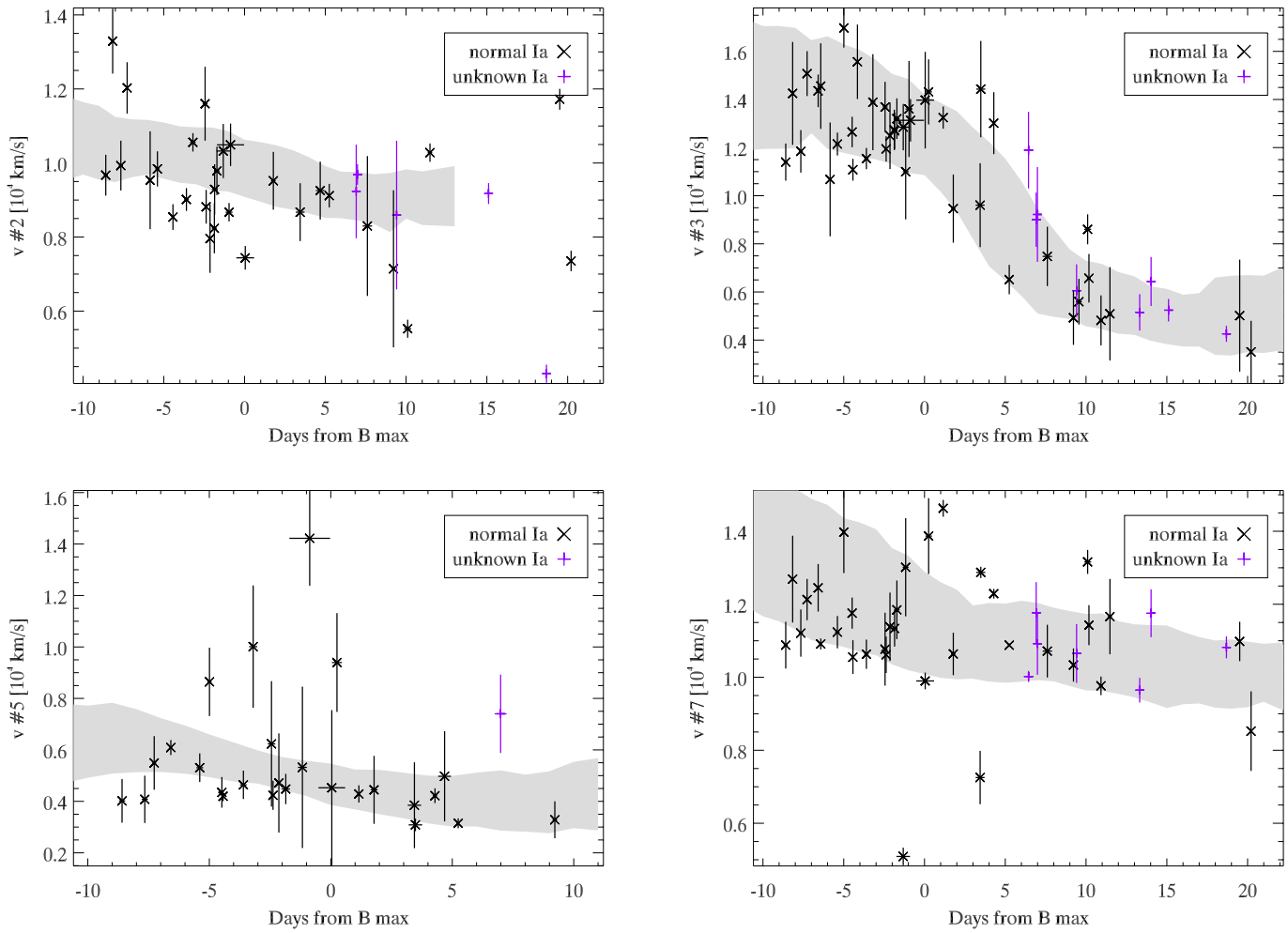

Fig. 10. Comparisons of line velocities (f2, f3, f5, f7) between the reference sample and the higher redshift SDSS spectra. The shaded band shows the one sigma contour for the normal SNe Ia in the reference sample.

Table 3. Correlations at peak brightness: r_S, Spearman correlation coefficient (number of standard deviations from null).

f	pEW – s	pEW – c	pEW – M	velocity – s	velocity – c	velocity – M
1	–	–	–	+0.19 (0.9)	−0.02 (0.1)	+0.05 (0.3)
2	−0.73 (4.8)	+0.19 (1.2)	+0.19 (1.3)	−0.00 (0.0)	+0.22 (1.3)	+0.01 (0.1)
3	+0.13 (0.9)	+0.34 (2.4)	+0.12 (0.8)	+0.16 (1.0)	+0.08 (0.5)	−0.15 (1.0)
4	−0.26 (1.8)	+0.42 (3.0)	−0.05 (0.4)	−0.36 (2.2)	+0.26 (1.6)	+0.13 (0.8)
5	−0.40 (2.9)	−0.18 (1.3)	+0.15 (1.1)	+0.19 (1.1)	−0.18 (1.1)	−0.13 (0.8)
6	−0.36 (2.4)	+0.02 (0.2)	−0.07 (0.4)	−0.02 (0.1)	+0.18 (1.1)	−0.14 (0.8)
7	−0.55 (3.8)	+0.15 (1.0)	−0.03 (0.2)	+0.07 (0.4)	+0.22 (1.3)	−0.02 (0.1)

Notes. At least 50 measurements used for each entry.

this method increases the probability of finding random correlations. For any set of three parameters, it will always be possible to find *some* correlation between two of these through restrictions of the third. For any correlating parameters we thus have to find the probability of finding such correlation(s) in random data. This is done through Monte Carlo simulations where we retain the epoch and indicator values and randomise the global property. We then search for correlations among epoch ranges exactly as for real data. This process is repeated 1000 times and the number of strongly correlating epoch ranges is saved for each. This result can be used to find the probability of finding as many strongly correlating epoch ranges by chance. For the correlations presented below, we find either zero or one out of 1000 iterations to yield as many correlated epoch ranges. We thus find that the probability that these correlations are completely random is equal to or smaller than 0.001.

The strongest correlation found was for the pEW for feature 2 and stretch when probing epochs right before maximum brightness. Depending on the epoch interval used, the Spearman correlation coefficient is about 0.6−0.7. It is a stable correlation in the sense that the coefficient remains large when the epoch interval is perturbed. A correlation between lightcurve width and feature 2 has been previously discussed by Bronder et al. (2008) and Arsenijevic et al. (2008).

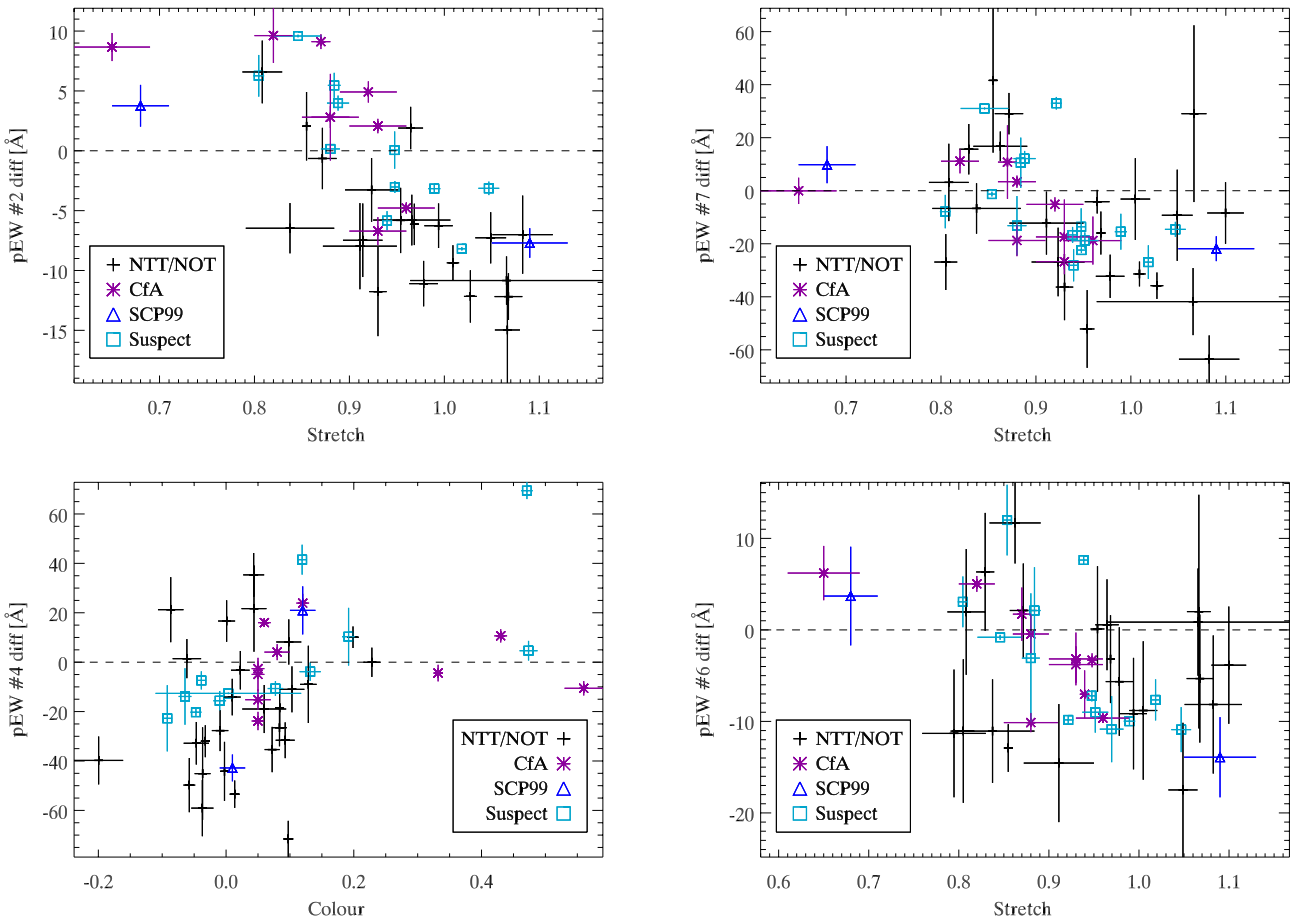

Fig. 11. These correlation studies show the measured pEW minus the expected pEW for the corresponding epoch for the full sample of normal SNe Ia vs. SALT lightcurve parameter (stretch, colour) for epoch ranges around peak (±3 days). Indicators chosen are the ones showing largest correlation for this epoch range.

The pseudo-equivalent width for feature 2 also seems to be correlated with the fitted SALT colour parameter, as shown in the left panel of Fig. 12, but mainly in the epochs just *after* peak. While SNe with SALT-$c \gtrsim 0.2$ do not appear to correlate with pEW, those below this rough limit seem to do. This could be interpreted as a sign of two different sources of reddening, where e.g. the highly reddened supernovae are dust extincted while most supernovae get their colour from some intrinsic property which is correlated with the strength of feature 2.

As was shown in Sect. 2.1, dust absorption according to Cardelli et al. (1989) would create a small pEW change in the *opposite* direction.

To probe the origin of these lightcurve correlations the same epoch ranges and indicators as displayed in Fig. 12 were examined using MLCS fit parameters. These results can be seen in Fig. 13. Correlation with lightcurve shape (Δ) is strong, while correlations with A_V are less clear. The correlation with Δ in the epoch range 0−8 is significant, while for the same epoch range, we find a correlation with SALT colour but only a weak correlation with stretch.

The origin of these correlations is further discussed in Sect. 6, where we focus on feature 2, Si II λ4000.

5.2.1. Summary: correlations with lightcurve parameters

Pseudo-equivalent widths, as measured in this sample, do correlate with lightcurve properties. We recreate strong linear correlations between f2-Si II λ4000 both with SALT stretch and MLCS Δ. Correlations with SALT colour were also found. In general we see weak correlations between most pEWs around lightcurve max and both stretch and colour in the sense that wider, bluer SNe have small equivalent widths.

5.3. Host-galaxy properties

It is well documented that star forming, late type galaxies host brighter SNe with wider lightcurve shape (Hamuy et al. 1996). Since correlations between lightcurve shape (stretch) and spectral indicators seem to be present in the data analysed, we expect the host-lightcurve correlation to propagate to a correlation between spectral and host galaxy properties. Recent studies have also found indications of correlations between host galaxy properties, like mass and metallicity, and supernova absolute magnitude that does *not* appear to be captured by lightcurve shape or colour (Gallagher et al. 2008; Kelly et al. 2010; Sullivan et al. 2010; Lampeitl et al. 2010b). It is thus of great interest to investigate if spectral indicators correlate with host galaxy properties, especially beyond what is related to lightcurve stretch.

All SN host galaxies were studied using the stellar formation code PEGASE. A description of this process can be found in Smith et al. (in prep.), and a comparison with lightcurve properties and Hubble diagram residuals in Lampeitl et al. (2010b). Here we use the estimated host galaxy type, host mass (in units of $M_\odot$) and specific star formation rate (sSFR; defined as the star

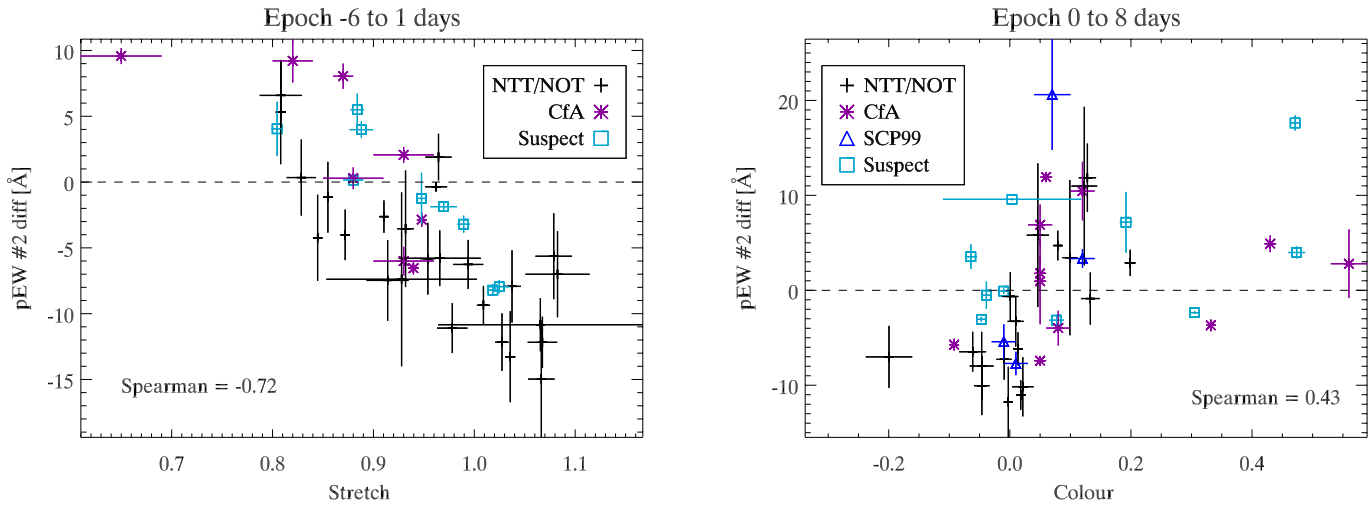

Fig. 12. These correlation studies show ΔpEW, the measured pEW minus the expected pEW for the corresponding epoch (for the full sample of normal SNe Ia), vs. SALT lightcurve parameter (stretch, colour) for different epoch intervals. These are given above each panel. The Spearman correlation coefficient is given in each plot. MC simulations show that the chance that these correlations are random consequences of a search through epoch ranges is one or less in 1000.

formation rate per stellar mass, yr) and compare with spectral indicators. Host type is defined based on specific star formation rate: type zero indicate no star formation, type one moderately star forming ($-12.5 < \log(\mathrm{sSFR}) < -9.5$) and type two star forming ($\log(\mathrm{sSFR}) > -9.5$). This parameter thus largely overlaps with sSFR, with the important exception that hosts with no star formation (type 0) are not displayed in the plots over sSFR values.

As previously, this search for correlations was performed using various epoch intervals, but with only SDSS NTT/NOT SNe. Once again, the largest $|r|$ were found when probing the second feature (Si II λ4000). When maximising the correlation for host mass and specific SFR, we obtained the epoch interval between 0 to 8 days past peak (which coincides with the epochs where a strong colour correlations is also seen).

We also minimize the KS probability for indicator measurements from SNe in different host galaxy types to originate from the same distribution. We do this through first compairing SNe from higly star-forming hosts (type 2) with remaining SNe (from host types 0 and 1), and then compairing SNe from non star-forming hosts (type 0) with star-forming (type 1 and 2). The epoch interval with *least* probability of distributions of pEWs from all host types being the same is epoch −9 to −2. These correlations are shown in Fig. 14.

Before lightcurve peak. The largest $|r|$ connection between lightcurve width and pEW was found to be for f2 during the epochs right before lightcurve peak. In the left panels of Fig. 14 we compare this feature with host galaxy properties. As can be expected, assuming a relation between stretch and host galaxy type, we see that actively star forming galaxies have lower pEW f2 values than passive galaxies. A possible alternative explanation is that SNe in passive galaxies (type 0) form a separate sub group: These all have large pEW f2 values, lower than average lightcurve widths and are only found in the very most massive host galaxies (as can be seen in the mid left panel of Fig. 14). More statistics is needed to determine whether such a subgroup exists, or if a continuous trend with host type or mass is present.

After lightcurve peak. We also found pEW f2 after lightcurve maximum to be related to host galaxy properties (right panels of Fig. 14). Lightcurve width and pEW f2 are correlated but not as strongly as before maximum. Instead we see a tentative correlation with SALT colour.

Most significant in this epoch range is what seems to be a linear correlation between sSFR and pEW f2. Alternatively, as for the epochs before peak, this could be explained using a subgroup of SNe, in this case consisting of blue SNe with small pEW f2 values and high specific star formation rate. This relationship is emphasised if we include host mass information; all SNe in this group have low host masses. Note that all SNe in actively star forming hosts (type 2) have smaller than average SALT-c lightcurve colours ($c < 0.05$), thus suggesting little dust extinction. Since we see a correlation with host galaxy mass, a random (uncorrelated) star formation rate would mean a correlated *specific* star formation rate (since this is the ratio between SFR and host mass). This clearly needs further study; we would expect SNe in small, star forming hosts to be more extincted.

5.3.1. Summary: correlations with host galaxy properties

Host galaxy properties and spectral indicators, mainly pEW f2, are clearly connected. Of special interest is whether further subgroups among normal SNe can be identified. Our results could be interpreted as a hint of the presence of *two subgroups*. One consisting of low stretch SNe with wide pEW f2, hosted by passive massive galaxies, and another consisting of blue SNe in actively star forming, low-mass galaxies.

6. Discussion

The discussion is split into a further examination of correlations in the Si II λ4000 region (Sect. 6.1), a search for signs of evolution with redshift (6.2), a discussion of host galaxy properties (6.3) and finally we revisit some systematic effects (6.4). This division does not mean that these topics are separate, they are rather closely related.

We use composite (average) spectra as a tool for searching for physical differences between subsets of SN Ia spectra.

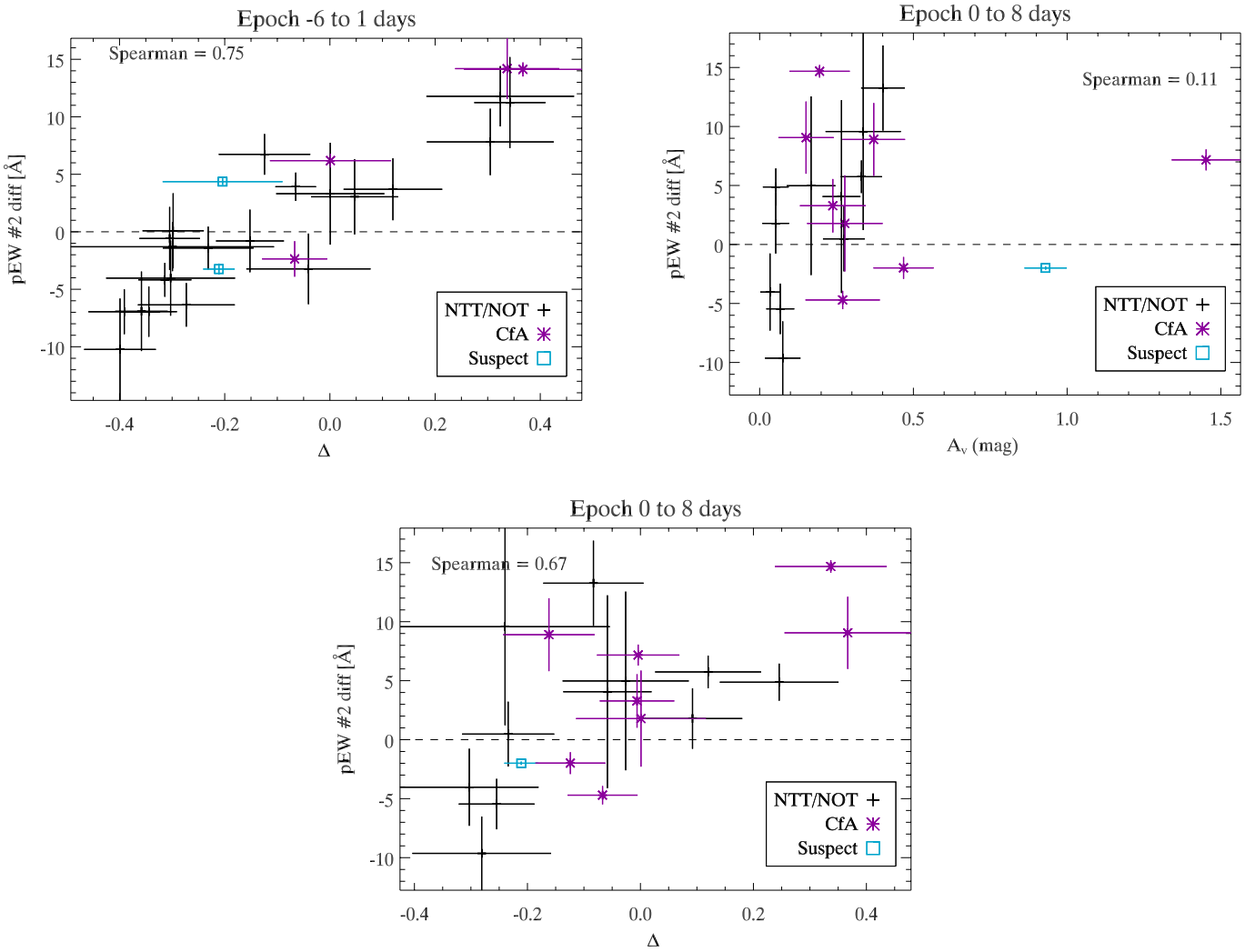

Fig. 13. These correlation studies show ΔpEW, the measured pEW minus the expected pEW (for the corresponding epoch for the full sample of normal SNe Ia), vs. MLCS2k2 lightcurve parameter (Δ, A_V) for different epoch intervals. These are given above each panel. The Spearman correlation coefficient is given in each plot. The epoch ranges were chosen to correspond to those used in Fig. 12. For the post lightcurve peak epoch range (0−8) we include correlations with both Δ and A_V.

Composite spectra can be normalised/created in a number of ways. This can make it hard to interpret the difference between two composite spectra in terms of physics or compare composite spectra created using different methods[5].

The composites shown here were created through scaling all spectra to have average $f_\lambda = 1$ in the studied region before combining. The uncertainties of the composites were then investigated through jackknife techniques. This simple procedure is sufficient since our purpose is to compare different subsets of spectra, not provide a "true" supernova composite.

6.1. Rest frame 4000–4500

This region roughly correspond to features two and three. The absorption feature at ~4050, here called f2 and usually attributed to Si II, has been shown to correlate with both luminosity and the stretch parameter in the sense of wider more luminous SNe having smaller equivalent width (Bronder et al. 2008; Arsenijevic et al. 2008). The same trend, using partially the same data, is seen clearly in this study using both SALT stretch (left top panel of Fig. 12) and MLCS Δ (left top panel of Fig. 13). We can further show that (i) the trend is *continous* with SALT-*s*/MLCS-Δ and (ii) strongest before lightcurve peak.

Including the broader absorption region around 4200 Å (here called f3, attributed to MgII amongst other ions), Garavini et al. (2007a) found a correlation between the "breaking point" of this feature and lightcurve width and Sullivan et al. (2009) found tentative signs of evolution, where high redshift objects have smaller equivalent widths. Bailey et al. (2009) used SNfactory data to look for the spectral regions most correlated with peak brightness; the best such was the ratio F(6420 Å)/F(4430 Å).

Finally one of the major spectral differences between normal and SN 1991bg-type SNe is the dominant Ti absorption at these wavelengths, even though these subluminous SNe are not included in this analysis.

This region is thus important both in order to understand and model supernova explosions as well as to make SNe better standard candles for use in cosmology. We will here try to probe the origin of the *pre-peak correlation with stretch* and the *post-peak correlation with colour* through comparisons of composite spectra.

[5] For example, Vanden Berk et al. (2001) show how continuum measurements on Quasar composite spectra change depending on combination method.

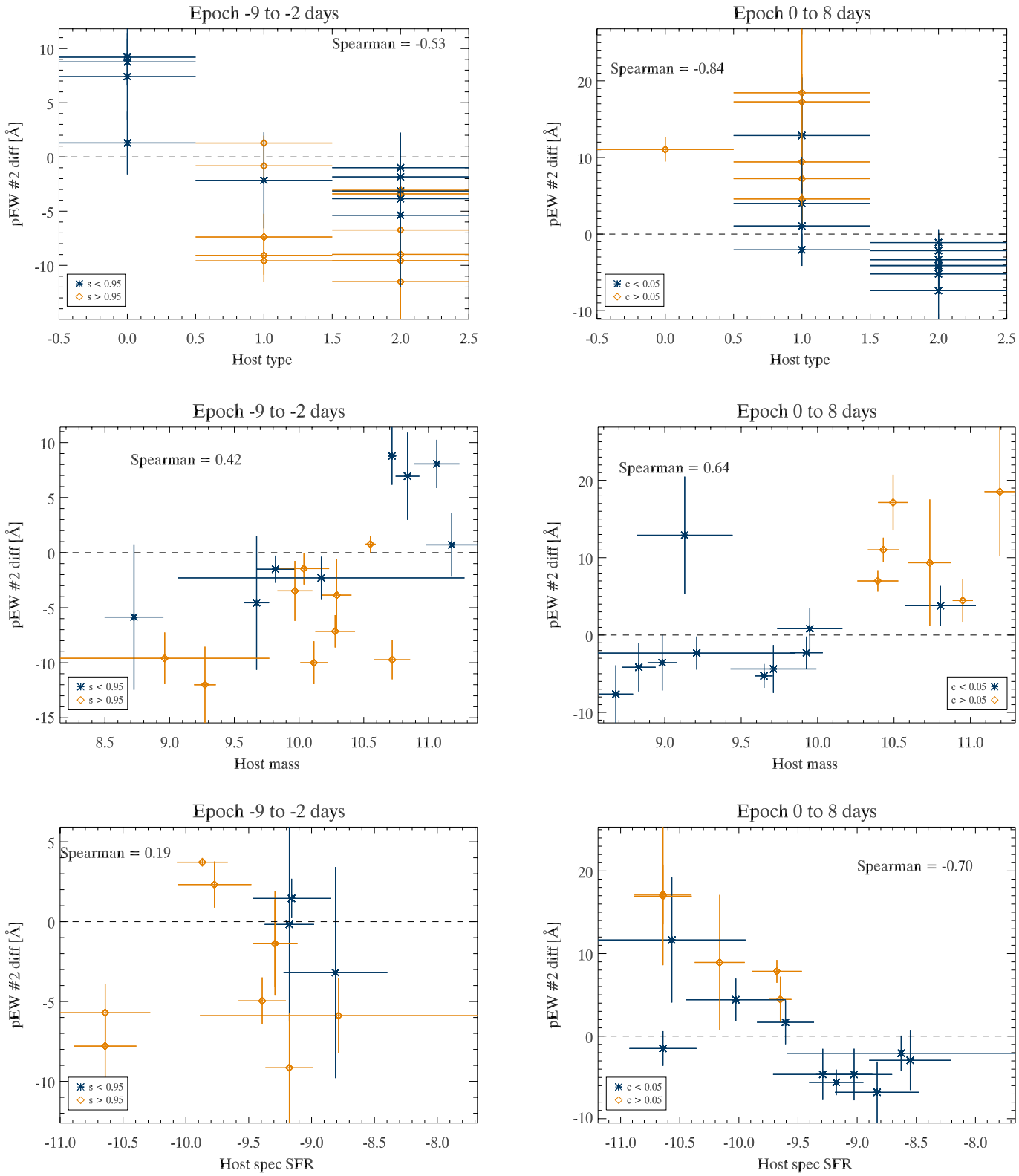

Fig. 14. Pseudo equivalent width of feature 2 compared with host galaxy properties. *Left panels*: pre peak epochs (−9 to 2) with colours marking low/high lightcurve stretch SNe. *Right panels*: post peak epochs (0 to 8) with colours marking low/high lightcurve colour SNe. *Top*: host type vs. pEW (0 not star forming, 1 moderately star forming, 2 highly star forming. *Middle*: Log of Host galaxy mass ($M_{\odot}$) vs. pEW. *Bottom*: Log specific start formation rate (log sSFR, yr^{-1}) vs. pEW.

Pre-peak stretch composite. All spectra contained in the epoch region between −6 and 1 (the region where the correlation with stretch was strongest) were included. Multiple spectra of single SNe were pre-combined. The sample was first divided into three stretch bins (low, intermediate and high). These composites can be seen in Fig. 15. Both the width and depth of the Si II λ4000 feature grow smaller with increasing stretch (exemplified by the almost nonexistent absorption for overluminous

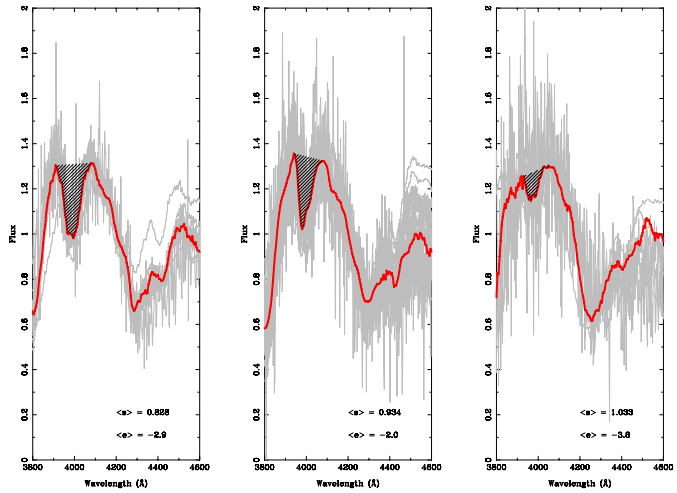

Fig. 15. Composite spectra constructed from all peak spectra (NTT/NOT as well as reference SNe), divided according to stretch. The average lightcurve stretch, *s*, is printed in each panel, increasing *from left to right*. The average epoch, *e*, is also included for each composite. The plots show both the composite (thick red) and individual (grey) spectra.

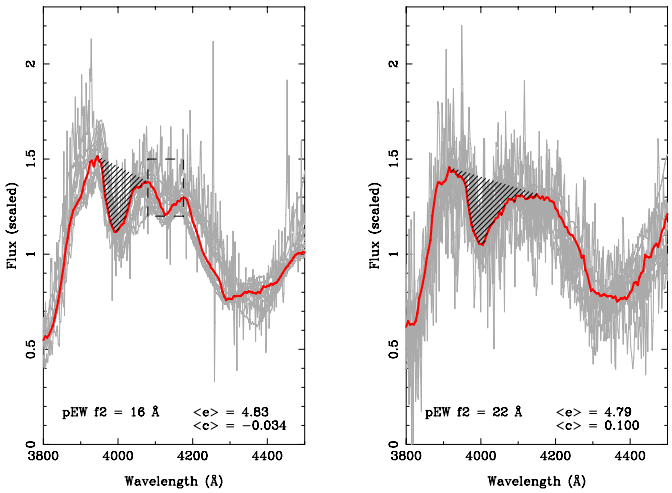

Fig. 16. Composite spectra constructed from all spectra with epochs in the range (3−8). *The left panel* composite is based on spectra with colour below average, *the right panel* one is based on spectra with colour above average. The plots show both composite (red) and individual (grey) spectra. The average SALT colours and epochs are printed for each composite, as well as the pEW for the indicated region. The dashed square marks a region where a small feature seems to exist only in the low colur sample (SALT $c < 0.03$), either because it is not resolved *or* because it is very rare among the higher colour SNe ($0.03 <$ SALT $c < 0.3$).

SN 1991T-like objects). Around the epoch of peak luminosity, the photosphere temperature and composition seem to be such that the ^{56}Ni yield, through the deposited energy, strongly affects Si II λ4000 ionisation and abundance, thereby causing a correlation between lightcurve width and Si II λ4000 depth.

As is discussed in Sullivan et al. (2009), changes in SN populations (Howell et al. 2007) will be seen as a change in average spectra with redshift. Bronder et al. (2008) argues that this pEW-lightcurve width correlation could be used to correct SN Ia lightcurve *instead* of using the lightcurve width. Our results, using a larger sample, support this conclusion. However, since photometry will be obtained for most SNe anyway and high S/N spectra in a small epoch range is needed, the practical use is limited.

Post-peak colour composite. Correlating spectroscopic indicators with lightcurve SALT colour yielded a statistically significant correlation between colour and Si II λ4000 pEW (using spectra obtained a few days after lightcurve peak). This correlation grows stronger if events with a colour above ∼0.2 are excluded. The need to remove highly reddened events could be explained if these are caused by a separate effect compared with moderately reddened SNe (e.g. circumstellar absorption). A correlation between spectral indicators and colour would be of great interest, as this would show that at least some part of the colour-luminosity relation seen in type Ia SNe originates in the SNe and not in any extinction external to the explosion.

In Fig. 16 we explore composite spectra constructed based on colour. Excluding very reddened eventes ($c > 0.3$) the average SALT colour for spectra with rest frame epochs in the (3−8) range is 0.03. As with stretch one composite spectra was created out of all spectra with colour below average and one out of all spectra with colour above average. The mean SALT colour values for the low colour composite is −0.03 and for the high colour composite 0.10.

The most interesting difference in Fig. 16 is a resolved small absorption at 4150 Å among the bluer SNe. This feature can not be seen in the corresponding redder colour composite. Various authors have suggested absorption by C II, Cr II, Co II or Fe III in this region, e.g. (Garavini et al. 2005; Branch et al. 2008; Scalzo et al. 2010) (as well as D. Sauer, priv. comm.). The average pEW will be smaller for the blue composite since the peak at 4070 Å provides a bluer feature bound; this bound will be set ∼4120 Å for the red (high colour) version. The average epochs for the two composites are very similar, and the effect is thus likely not created by epoch variations[6]. We finally note that the blue edge of the 3900 Å peak is slightly weaker in the lower than average colour composite (left panel Fig. 16).

Extinction by dust could, especially in the presence of noise, cause a pEW correlation with SALT-c or MLCS-A_V as follows: highly extincted, i.e., highly reddened SNe, have a large fraction of the flux around 4000 Å absorbed. The relative S/N levels will thus be smaller for redder SNe, which could make it impossible to resolve the small 4150 Å absorption. This effect would be more significant for SNe with already low S/N.

While it is clear that the composites differ with respect to the 4150 Å absorption, we cannot further distinguish between: (i) random small sample effects (ii) lower S/N preventing resolution of the small dip and (iii) a difference in the nature of the explosion correlated with SALT colour. The last alternative is intriguing, and strengthens the interest in using spectral indicators to disentangle the dependence of supernova properties on colour.

6.2. Evolution

Evolution of SNe Ia is a "thorny" issue; it is hard to make firm predictions or document that SN properties have "evolved". From a theoretical point of view, changing metallicity (and other parameters changing with time, like galaxy ages) could have an impact on SN Ia progenitor systems, but the details remain

[6] Feature 3 also show some correlation with colour in the same epoch range. Since these features share a border this correlation can very well be caused by flux change around 4100 Å.

largely unknown. Previous work on SN Ia indicates that their properties appear to vary depending on the surrounding environment (Gallagher et al. 2008; Sullivan et al. 2010; Lampeitl et al. 2010b) and redshift (Howell et al. 2007). So far these effects are interpreted as due to population evolution (a larger fraction of "prompt" high stretch objects at higher redshifts, Mannucci et al. 2005).

Such evolution would not per se imply any fundamental problems for SN cosmology. However, if spectral evolution *not* captured in lightcurve shape fits would be detected, this could create a cosmological parameter bias since these spectral changes are likely to affect luminosity. We thus need to show that we understand such changes.

Both the ESSENCE (Foley et al. 2008) and SNLS (Balland et al. 2009; Sullivan et al. 2009) collaborations have reported indications of evolution, or systematic differences in redshift binned composite spectra. Both groups use samples where the average lightcurve width increases with redshift. Based on the lightcurve shape correlations found above, we would thus expect decreasing equivalent widths with redshift. This agrees qualitatively with the differences found by both groups.

6.2.1. The pEW-deficit subsample

As was discussed in Sect. 4.2, the deviations between the reference and NTT/NOT SNe can be attributed to a set of SNe with lower pseudo-equivalent widths than the non-peculiar reference SNe. These were collected in a *pEW-deficit* sample. We will here study why these NTT/NOT SNe deviate and whether this is a sign for SN Ia evolution. As our basic tool we create composite spectra of *deficit* SNe and compare with composite spectra based on normal non-deficit NTT/NOT SNe.

As can be seen in Fig. 8, most spectra with low pEW f2 can be found *before* lightcurve peak while the deviations in f4 are most clear *after* peak. We therefore make two separate studies: in Fig. 17 we compare spectra with deficit pEW f2 in the epoch range −5 to 0 with non-*f2deficit* spectra in this epoch range. In Fig. 18 we compare spectra with deficit pEW f4 in the epoch range 0 to 5 with non-*f4deficit* spectra[7]. In each figure we also include the mean and dispersion of a number of properties for each subset. These include both lightcurve properties and estimates for possibly systematic effects like slit loss and host galaxy contamination (see Östman et al. 2010, regarding these estimates). We caution that most composites consist of comparably few objects (∼10), and are thus sensitive to random fluctuations.

Description of (physical) differences. The mean spectra are similar in both cases, except for some limited regions. These are marked with black arrows. Starting with Fig. 17 (the pEW f2 deficit before peak brightness) the *deficit* composite has more flux (less absorption) at the silicon lines Si II λ4000 (f2) and Si II λ5800 (f5), as well as at 4400 Å.

In Fig. 18 (pEW f4 deficit after peak brightness) we find more flux (less absorption) in the *normal* composite both at 4150 Å and 4500 Å.

Do the differences agree with lightcurve correlations? We can understand most of the observed differences seen based on the correlations between pseudo-Equivalent widths and lightcurve properties. The pEW f2 deficit SNe in Fig. 17 have, on average, higher stretch (1.03) than the normal set (0.92). As was seen above, pEW f2/Si II λ4000 has a strong negative correlation with stretch. The same is true for Si II λ5800 (see Nugent et al. 1995). Interestingly, the region around 4400 Å show a similar variation as the Si lines. This region was one of the flux ratio "legs" used by Bailey et al. (2009) to standardize SNe Ia (as an alternative to lightcurve width). This suggests that the same physical process is responsible for the absorption seen here as at the Si lines.

The f4 composites in Fig. 18 have a (small) difference in average stretch, but also in SALT colour: the average colour for the deficit sample is −0.02 while it is 0.03 for the normal sample.

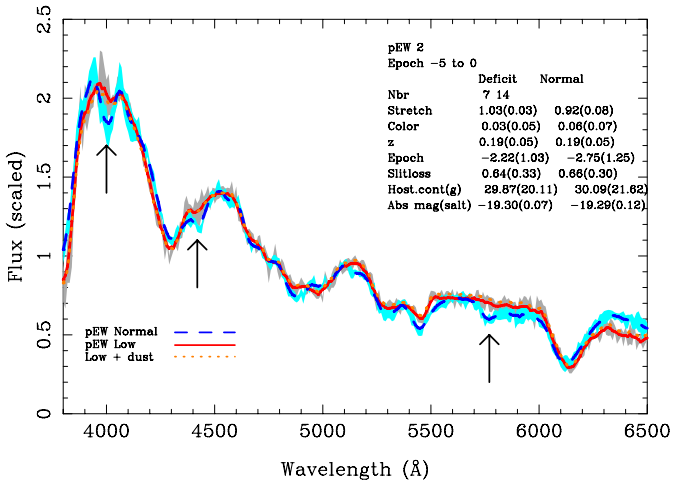

Fig. 17. *Pre peak, f2 deficit vs. normal*: composite spectra of "reference normal" SNe (dashed blue) compared with pEW-deficit SNe (solid red) in the epoch range −5 to 0 days past peak brightness. The shaded regions correspond to jackknife dispersion (light blue for normal, grey for deficit). The dotted orange line corresponds to the deficit composite with Cardelli et al. (1989) dust applied that matches the colour difference. The arrows indicate features discussed in the text. Mean properties of the composites are stated in the figure.

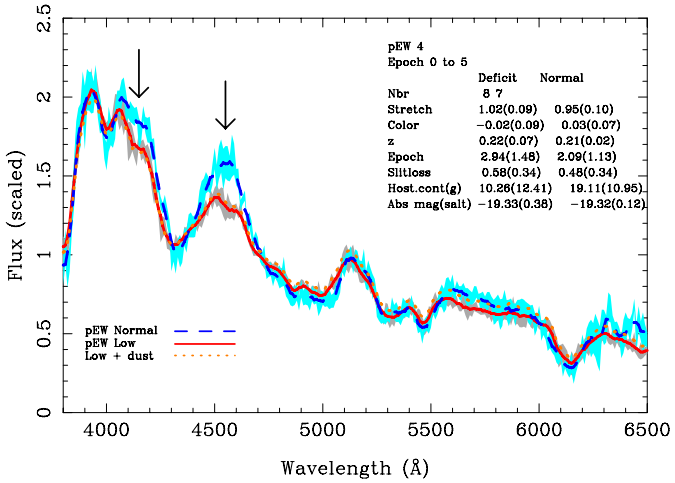

Fig. 18. *Post peak, f4 deficit vs. normal*: composite spectra of "reference normal" SNe (dashed blue) compared with pEW-deficit SNe (solid red) in the epoch range 0 to 5 days past peak brightness. The shaded regions correspond to jackknife dispersion (light blue for normal, grey for deficit). The dotted orange line corresponds to the deficit composite with Cardelli et al. (1989) dust applied matching the colour difference. The arrows indicate features commented on in the text. Mean properties of the composites are stated in figure.

[7] Spectra of three SNe (17880, 16215 and 18466) were too deformed (reddening/slit loss) to be used in a composite and were removed from the analysis.

The differences in colour is smaller than the dispersion, but does agree in direction with what we expect form the tentative colour correlation seen in Table 3. As the NTT/NOT SNe have a lower mean colour this could explain why SNe at higher redshifts seem to have smaller pEW f4[8].

We also find a significant difference at 4130 Å, possibly related to the discussion (also including non-SDSS spectra) in Sect. 6.1 and Fig. 16. More flux is absorbed among low-reddened objects.

We finally note that some pEW selected subsamples have a smaller absolute magnitude dispersion (restframe *B* band). Sample sizes are too small to properly evaluate this effect.

Could the differences be caused by systematic effects? Systematic effects such as inaccurate correction of host galaxy contamination, slit loss or dust extinction could significantly affect spectral comparisons.

To study dust extinction we have applied Cardelli et al. (1989) type dust matching the difference in SALT colour to the (less reddened) *deficit* composite (dotted orange line in Figs. 17 and 18). In none of the cases does this approach create a better match to the normal set. Standard dust could thus not by itself create the observed differences.

In each figure we have also included mean and dispersion for our (conservatively) *estimated* slit loss and host contamination for each subset. Slit loss is defined as the fractional flux loss at 4000 Å (observed frame), host galaxy contamination as the fraction of galaxy flux in the observed *g* band *before* host galaxy subtraction. Slit loss values are consistent among all subsets. Host contamination levels are almost identical for the pEW f2 samples shown in Fig. 17.

For the pEW f4 divided subsets in Fig. 18 the mean contamination level is lower for the *deficit* sample (∼10%), but it is still comparably low for the reference SNe (∼19)%). It is very unlikely that this would cause a host contamination systematic difference since (i) the spectral composite differences seen are localized to small wavelength regions and (ii) it is the less contaminated objects that seem to deviate.

In summary, we find no reasonable combination of systematic effects that could create the *deficit* subsample.

Are the pEW deficit SNe "peculiar"? The deficit NTT/NOT SNe were chosen since they do not correspond to *normal* reference SNe Ia. It is natural to ask whether they instead correspond to SNe Ia locally defined as peculiar. None of them seem to be "very" odd, in the sense of SN 2000cx or SN 1991T. But they do correspond to several other slightly peculiar *Shallow Silicon* (SS) SNe, like SN 1999aw, SN 1999bp and SN 1999bn (See Branch et al. 2008, for a definition of SS). The deficit spectra have, in general, wide lightcurves and small "shallow" silicon features.

In total we have 21 SNe belonging to either the f2 or the f4 deficit subgroups. Among these we find three NTT/NOT SNe that can be classified as SS SNe (15132, 17497 and 19899). Seven (out of 21) SNe have spectra good enough to be classified as *not* of this subtype, leaving 14 SNe as possibly peculiar. We thus have between 3 and 14 SNe that would have been identified as peculiar if observed locally. In total (deficit *and* normal) we have 41 spectra in this epoch range, which translates into a fraction of SS SNe between 7% (3 out of 41) and 32% (14 out of 41). Li et al. (2010) found that 18% of all SNe in a luminosity limited sample was of the SN1991T subtype but that it gets significantly harder to identify these without early spectra.

Summary: evolution. The "deviations" between the NTT/NOT data set and the normal reference set can be explained through a combination of two (connected) effects:

- A fraction of "borderline" peculiar SNe, mainly similar to Shallow Silicon SNe, that would have been identified as such if obsereved locally and thus do not exist in the reference sample of normal SNe.
- SN features change with lightcurve parameters. Sets with different lightcurve parameters will thus have different spectral properties.

6.2.2. Sensitivity to evolution models

While we cannot exactly determine our sensitivity to (an unknown) spectral evolution, we have simulated how well we would have detected some models of evolution. This process is further described in Appendix A. These simulations used all property distributions in the NTT/NOT sample and determined how well we would detect *changing SNe subtype distributions*, that is if the fraction of evolved SN increased with redshift. We conclude that most of the models studied should have been discovered at least at low significance ($\sim 2\sigma$), using one or more indicators and possibly removing high bias events. These models are, however, not realistic. It is possible that an increased fraction of "deficit" SNe is a sign of evolving subtype distribution, but if so this does not limit the use of SNe Ia as standard candles (since these SNe seem to follow the same luminosity-width relation as other SNe Ia).

6.3. Host galaxy properties

Different galaxy types give rise to different type Ia SN populations. First, the distribution of lightcurve parameters differ. Second, as indicated by Kelly et al. (2010); Sullivan et al. (2010) and Lampeitl et al. (2010b), Hubble diagram residuals seem to correlate with host types. However, it is still not clear how strong these effects are or the causes.

The comparisons between Si II λ4000 and host galaxy properties could help clarify these questions. As is discussed in Sect. 5.3 we see indications of relations between spectral indicators and host galaxy properties.

For the epochs after lightcurve peak, we see signs of correlation with both host mass and specific star formation rate. The measurements could also be interpreted as belonging to different subtypes of SNe Ia (e.g. a subset of SNe produced in low mass hosts with high sSFR whose spectra after peak show very small Si II λ4000 values).

Correlations with host mass could be present also for pre-max spectral epochs. This is best seen by separating low and high lightcurve stretch SNe.

We have also compared the host galaxy types with the subset of SNe defined as (possible) shallow silicon (SS) SNe. We find that all clear SS SNe originate in actively star forming galaxies

[8] We can make a *very speculative* extended comparison with the Bailey et al. (2009) results: if we assume that lightcurve width causes spectral differences as seen in Fig. 17 and reddening causes spectral differences as seen in Fig. 18 and we want to find one wavelength where flux correlate *both* with lightcurve width and reddening, we are led to the small overlap region at ∼4400 Å. Bailey et al. (2009) see most significant correlation at 4430 Å.

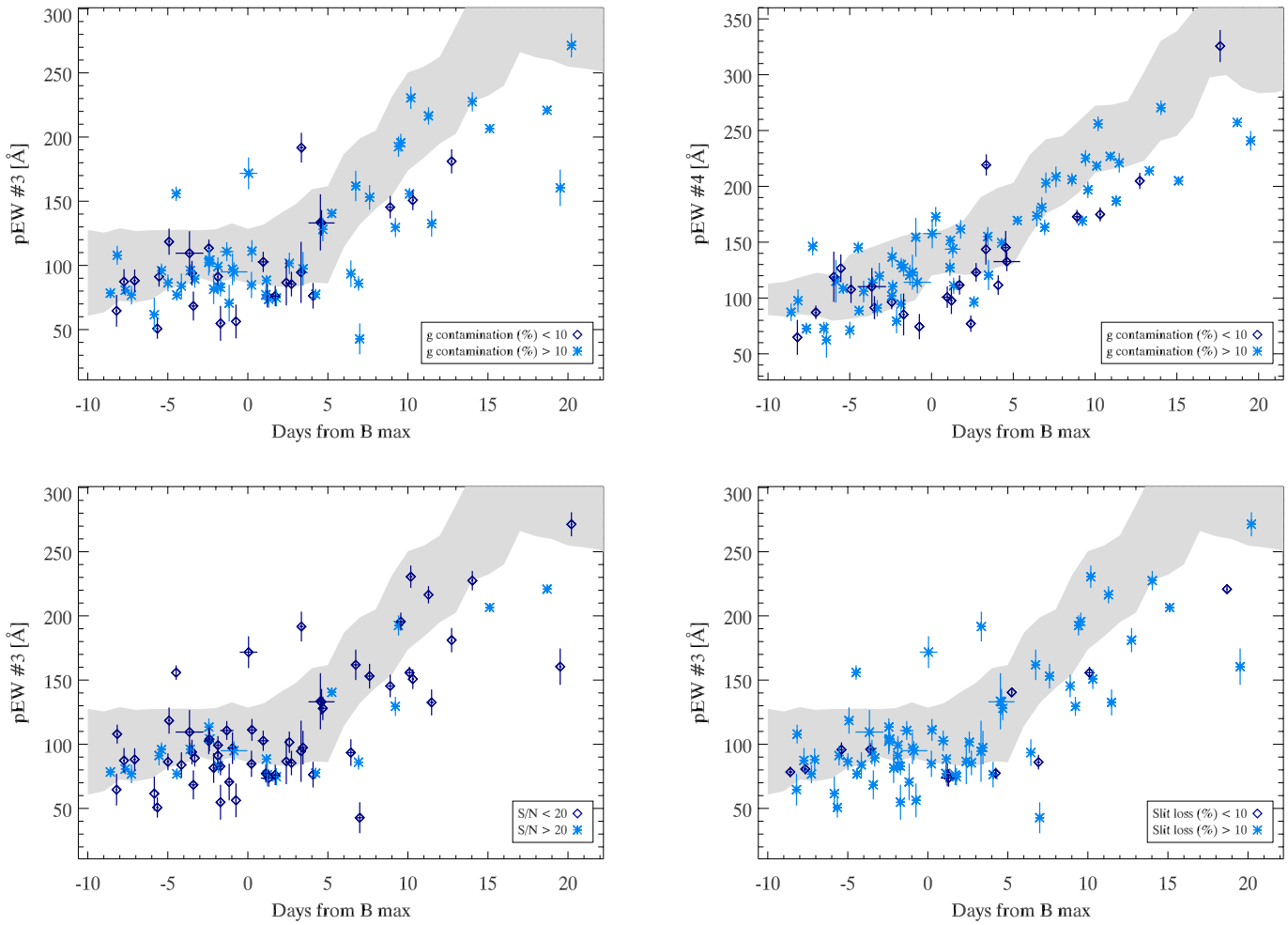

Fig. 19. Study of systematic effects: Each panel highlight pEW measurements possibly affected by systematic effects. *Top left*: feature 3 highlighting low contamination events. *Top right*: feature 4 highlighting low contamination events. *Bottom left*: feature 3 highlighting high S/N SNe. *Bottom right*: feature 3 highlighting low slit loss SNe. No major deviations in subsets with possible systematic errors are detected.

(type 2) as well as three out of four likely SS SNe. These six SNe constitute almost half of all the 13 SNe with host galaxies of type 2 (with spectra in the −5 to 5 epoch range). Considering the SNe too noisy to be identified as belonging to a subtype this implies that *half or more of all SNe in our sample from actively star forming galaxies are similar to Shallow Silicon SNe*. We also note that these SNe tend to have blue SALT lightcurve colours and originate in lower mass host galaxies.

6.4. Systematic effects

We have studied several possible systematic effects. In Fig. 19 we show some sample indicator measurements with NTT/NOT SNe divided into subsamples according to possibly systematic effects. For example, if host galaxy contamination would yield a systematic bias we would expect low contaminated SNe to differ from the high contamination set. We did not detect any such differences or signs of systematic differences.

Use of local templates. We make use of our knowledge of local SNe and SN templates in a number of different ways. This includes both the host-galaxy subtraction method used here and identification of SNe using templates (e.g. using software like SNID).

This approach is clearly not ideal and creates tension when probing for evolution with redshift. A few items to note regarding this:

- For moderate evolution, local templates should provide a fair match, and we should be able to accurately type SNe and extract clean spectra. It would be a striking coincidence if the evolution could be completely masked through varying the three galaxy eigenspectra used to model the galaxy. The coefficients of the fit are strongly over-determined by the number of wavelength bins fitted.
- It is significantly harder to identify completely new subtypes among low S/N distant SNe. While this would be very interesting it is not within the scope of this study.
- Most cosmological surveys use an identification mechanism relying on known templates to select the SNe to include in samples for cosmological fits.
- The synthetic spectra discussed in Appendix A are constructed from SN spectra which differ from the templates used in the host subtraction. Simulations show that we can still get correct indicator measurements after subtractions.

We thus conclude that the use of SN templates is not a fundamental objection when searching for evolution among SNe Ia used for cosmological studies. Our general conclusions would not have changed if only objects with small contamination were

included, see Fig. 19, although they would have had smaller statistical significance.

Noise and slit loss. Two further possible systematic effects are noise and slit loss. The possible bias effects when comparing high and low S/N data should not be underestimated. To probe these effects, the NTT/NOT sample was split into high/low S/N and high/low slit loss samples and the results compared. In Fig. 19 we show these for feature 3. No significant bias was detected. Simulation results show that we can adjust indicator errors according to noise levels.

However, we note that noise can still limit our ability to determine whether spectral differences are "real". In Sect. 6.1 we discussed whether higher noise levels in more reddened SNe could hide small spectral features seen among less reddened SNe.

Selection effects. The NTT/NOT sample was obtained as part of the SDSS-II Supernova Survey, a rolling search. Very faint targets were usually scheduled for typing at larger aperture telescopes. Even though the NTT/NOT sample has a normal distribution of lightcurve parameters, it is thus possible that these SNe are not representable for the SN Ia population as a whole (e.g. missing some faint objects). We have not attempted a full study of the completeness of the NTT/NOT sample.

The reference sample is very inhomogeneous. These SNe were not observed as part of a rolling survey, and more or less peculiar objects are over represented. Also, since multiple spectra exist of many objects, these objects will carry larger weights.

Finally, the distribution of epoch and colour differ between the samples. We can thus not expect full agreement between the samples.

As we conclude above the differences between the reference and NTT/NOT sample can be explained by a fraction of semi-peculiar Shallow Silicon SNe. To properly identify these objects, multiple high S/N spectra at early epochs are needed; it is thus not surprising that these are identified in low-z data but not in the NTT/NOT sample.

7. Conclusions

We have measured both pseudo-Equivalent widths and line velocities of individual optical spectra observed at the NTT and NOT as part of the SDSS-II Supernova Survey. These spectra cover the redshift range 0.05−0.3. Our spectra were compared with a low-redshift sample to probe a possible evolution between local SNe and SNe at cosmological redshifts. The samples were then combined and all SNe were used to investigate possible correlations with lightcurve properties.

The differences between reference and moderate redshift SNe can be well described by a fraction (∼20%) of slightly peculiar, possibly Shallow Silicon, SNe Ia.

The linear correlation between Si II λ4000 pseudo Equivalent-width and lightcurve shape is very significant, both when using SALT stretch and MLCS Δ parameterisation. We also found correlations between this feature and SALT lightcurve colour (particularly if highly reddened events are excluded) in spectra observed roughly during the first week after lightcurve peak. This could be an effect from intrinsic colour dependence or a sign of different noise levels. In this epoch range, Si II λ4000 correlates with MLCS Δ, but we also see a faint correlation with MLCS A_V for NTT/NOT SNe. Further studies have to conclude whether an intrinsic physical correlation with reddening exist.

We do not see any significant correlation between spectral properties and absolute magnitude, but we do find a smaller magnitude dispersion among SNe subsamples defined through pEW.

We also found connections between host galaxy properties and spectral indicators. As for the correlations with lightcurve parameters, these seem strongest for Si II λ4000. Future studies are needed to confirm whether these are real, and whether they, in turn, derive from lightcurve parameters. The correlations could be explained by a subset of SNe with weak Si II λ4000 appearing in hosts with low mass and high star formation.

Acknowledgements. We thank the anonymous referee for valuable comments. We also thank Ryan J. Foley for helpful discussions. Funding for the Sloan Digital Sky Survey (SDSS) has been provided by the Alfred P. Sloan Foundation, the Participating Institutions, the National Aeronautics and Space Administration, the National Science Foundation, the US Department of Energy, the Japanese Monbukagakusho, and the Max Planck Society. The SDSS Web site is http://www.sdss.org/. The SDSS is managed by the Astrophysical Research Consortium (ARC) for the Participating Institutions. The Participating Institutions are The University of Chicago, Fermilab, the Institute for Advanced Study, the Japan Participation Group, The Johns Hopkins University, Los Alamos National Laboratory, the Max-Planck-Institute for Astronomy (MPIA), the Max-Planck-Institute for Astrophysics (MPA), New Mexico State University, University of Pittsburgh, Princeton University, the United States Naval Observatory, and the University of Washington. The paper is partly based on observations made with the Nordic Optical Telescope, operated on the island of La Palma jointly by Denmark, Finland, Iceland, Norway, and Sweden, in the Spanish Observatorio del Roque de los Muchachos of the Instituto de Astrofisica de Canarias. The data have been taken using ALFOSC, which is owned by the Instituto de Astrofisica de Andalucia (IAA) and operated at the Nordic Optical Telescope under agreement between IAA and the NBI. This paper is partly based on observations collected at the New Technology Telescope (NTT), operated by the European Organisation for Astronomical Research in the Southern Hemisphere, Chile. The Oskar Klein Centre is funded by the Swedish Research Council. The Dark Cosmology Centre is funded by the Danish National Research Foundation. We thank the Swedish Foundation for International Cooperation in Research and Higher Education (STINT) for financial support.

References

Altavilla, G., Fiorentino, G., Marconi, M., et al. 2004, MNRAS, 349, 1344
Altavilla, G., Stehle, M., Ruiz-Lapuente, P., et al. 2007, A&A, 475, 585
Amanullah, R., Lidman, C., Rubin, D., et al. 2010, ApJ, 716, 712
Anupama, G. C., Sahu, D. K., & Jose, J. 2005, A&A, 429, 667
Arsenijevic, V., Fabbro, S., Mourão, A. M., & Rica da Silva, A. J. 2008, A&A, 492, 535
Astier, P., Guy, J., Regnault, N., et al. 2006, A&A, 447, 31
Bailey, S., Aldering, G., Antilogus, P., et al. 2009, A&A, 500, L17
Balland, C., Baumont, S., Basa, S., et al. 2009, A&A, 507, 85
Barbon, R., Benetti, S., Rosino, L., Cappellaro, E., & Turatto, M. 1990, A&A, 237, 79
Benetti, S., Meikle, P., Stehle, M., et al. 2004, MNRAS, 348, 261
Benetti, S., Cappellaro, E., Mazzali, P. A., et al. 2005, ApJ, 623, 1011
Blondin, S., Dessart, L., Leibundgut, B., et al. 2006, AJ, 131, 1648
Blondin, S., & Tonry, J. L. 2007, ApJ, 666, 1024
Branch, D., Garnavich, P., Matheson, T., et al. 2003, AJ, 126, 1489
Branch, D., Dang, L. C., Hall, N., et al. 2006, PASP, 118, 560
Branch, D., Jeffery, D. J., Parrent, J., et al. 2008, PASP, 120, 135
Bronder, T. J., Hook, I. M., Astier, P., et al. 2008, A&A, 477, 717
Cappellaro, E., Patat, F., Mazzali, P. A., et al. 2001, ApJ, 549, L215
Cardelli, J. A., Clayton, G. C., & Mathis, J. S. 1989, ApJ, 345, 245
Cristiani, S., Cappellaro, E., Turatto, M., et al. 1992, A&A, 259, 63
Elias-Rosa, N., Benetti, S., Cappellaro, E., et al. 2006, MNRAS, 369, 1880
Ellis, R. S., Sullivan, M., Nugent, P. E., et al. 2008, ApJ, 674, 51
Folatelli, G. 2004, New Astron. Rev., 48, 623
Foley, R. J., Filippenko, A. V., Aguilera, C., et al. 2008, ApJ, 684, 68
Frieman, J. A., Bassett, B., Becker, A., et al. 2008, AJ, 135, 338
Gallagher, J. S., Garnavich, P. M., Caldwell, N., et al. 2008, ApJ, 685, 752
Garavini, G., Folatelli, G., Goobar, A., et al. 2004, AJ, 128, 387
Garavini, G., Aldering, G., Amadon, A., et al. 2005, AJ, 130, 2278
Garavini, G., Folatelli, G., Nobili, S., et al. 2007a, A&A, 470, 411

Garavini, G., Nobili, S., Taubenberger, S., et al. 2007b, A&A, 471, 527
Garnavich, P. M., Bonanos, A. Z., Krisciunas, K., et al. 2004, ApJ, 613, 1120
Gerardy, C. L. 2005, in 1604−2004: Supernovae as Cosmological Lighthouses, ed. M. Turatto, S. Benetti, L. Zampieri, & W. Shea, ASP Conf. Ser., 342, 250
Gómez, G., & López, R. 1998, AJ, 115, 1096
Gomez, G., Lopez, R., & Sanchez, F. 1996, AJ, 112, 2094
Goobar, A. 2008, ApJ, 686, L103
Gunn, J. E., Carr, M., Rockosi, C., et al. 1998, AJ, 116, 3040
Guy, J., Astier, P., Nobili, S., Regnault, N., & Pain, R. 2005, A&A, 443, 781
Guy, J., Astier, P., Baumont, S., et al. 2007, A&A, 466, 11
Hachinger, S., Mazzali, P. A., Tanaka, M., Hillebrandt, W., & Benetti, S. 2008, MNRAS, 389, 1087
Hamuy, M., Phillips, M. M., Suntzeff, N. B., et al. 1996, AJ, 112, 2391
Hamuy, M., Maza, J., Pinto, P. A., et al. 2002, AJ, 124, 417
Hicken, M., Garnavich, P. M., Prieto, J. L., et al. 2007, ApJ, 669, L17
Hicken, M., Wood-Vasey, W. M., Blondin, S., et al. 2009, ApJ, 700, 1097
Holtzman, J. A., Marriner, J., Kessler, R., et al. 2008, AJ, 136, 2306
Hook, I. M., Howell, D. A., Aldering, G., et al. 2005, AJ, 130, 2788
Howell, D. A., Sullivan, M., Conley, A., & Carlberg, R. 2007, ApJ, 667, L37
Hsiao, E. Y., Conley, A., Howell, D. A., et al. 2007, ApJ, 663, 1187
Jha, S., Garnavich, P., Challis, P., Kirshner, R., & Berlind, P. 1999, IAU Circ., 7149, 2
Jha, S., Riess, A. G., & Kirshner, R. P. 2007, ApJ, 659, 122
Kelly, P. L., Hicken, M., Burke, D. L., Mandel, K. S., & Kirshner, R. P. 2010, ApJ, 715, 743
Kessler, R., Becker, A. C., Cinabro, D., et al. 2009a, ApJS, 185, 32
Kessler, R., Bernstein, J. P., Cinabro, D., et al. 2009b, PASP, 121, 1028
Kinney, A. L., Calzetti, D., Bohlin, R. C., et al. 1996, ApJ, 467, 38
Kotak, R., Meikle, W. P. S., Pignata, G., et al. 2005, A&A, 436, 1021
Kowalski, M., Rubin, D., Aldering, G., et al. 2008, ApJ, 686, 749
Krisciunas, K., Hastings, N. C., Loomis, K., et al. 2000, ApJ, 539, 658
Krisciunas, K., Suntzeff, N. B., Candia, P., et al. 2003, AJ, 125, 166
Krisciunas, K., Garnavich, P. M., Stanishev, V., et al. 2007, AJ, 133, 58
Lampeitl, H., Nichol, R. C., Seo, H., et al. 2010a, MNRAS, 401, 2331
Lampeitl, H., Smith, M., Nichol, R. C., et al. 2010b, ApJ, 722, 566
Lentz, E. J., Baron, E., Branch, D., Hauschildt, P. H., & Nugent, P. E. 2000, ApJ, 530, 966
Leonard, D. C. 2007, in Supernova 1987A: 20 Years After: Supernovae and Gamma-Ray Bursters, ed. S. Immler, K. Weiler, & R. McCray, Am. Inst. Phys. Conf. Ser., 937, 311
Li, W. D., Qiu, Y. L., Qiao, Q. Y., et al. 1999, AJ, 117, 2709
Li, W., Filippenko, A. V., Gates, E., et al. 2001, PASP, 113, 1178
Li, W., Leaman, J., Chornock, R., et al. 2010 [arXiv:1006.4612]
Maeda, K., Benetti, S., Stritzinger, M., et al. 2010, Nature, 466, 82
Mannucci, F., Della Valle, M., Panagia, N., et al. 2005, A&A, 433, 807
Matheson, T., Kirshner, R. P., Challis, P., et al. 2008, AJ, 135, 1598
Mazzali, P. A., Lucy, L. B., Danziger, I. J., et al. 1993, A&A, 269, 423
Mazzali, P. A., Danziger, I. J., & Turatto, M. 1995, A&A, 297, 509
Nobili, S., & Goobar, A. 2008, A&A, 487, 19
Nordin, J., Goobar, A., & Jönsson, J. 2008, J. Cosmol. Astro-Part. Phys., 2, 8
Nugent, P., Phillips, M., Baron, E., Branch, D., & Hauschildt, P. 1995, ApJ, 455, L147
Nugent, P., Kim, A., & Perlmutter, S. 2002, PASP, 114, 803
Östman, L., Nordin, J., Goobar, A., et al. 2010, A&A, 526, A28
Pastorello, A., Mazzali, P. A., Pignata, G., et al. 2007, MNRAS, 377, 1531
Patat, F., Benetti, S., Cappellaro, E., et al. 1996, MNRAS, 278, 111
Perlmutter, S., Aldering, G., Goldhaber, G., et al. 1999, ApJ, 517, 565
Phillips, M. M., Krisciunas, K., Suntzeff, N. B., et al. 2006, AJ, 131, 2615
Phillips, M. M., Li, W., Frieman, J. A., et al. 2007, PASP, 119, 360
Pignata, G., Benetti, S., Mazzali, P. A., et al. 2008, MNRAS, 388, 971
Press, W. H., Teukolsky, S. A., Vetterling, W. T., & Flannery, B. P. 1992, Numerical recipes in FORTRAN, The art of scientific computing, ed. W. H. Press, S. A. Teukolsky, W. T. Vetterling, & B. P. Flannery
Quimby, R., Höflich, P., Kannappan, S. J., et al. 2006, ApJ, 636, 400
Quimby, R., Höflich, P., & Wheeler, J. C. 2007, ApJ, 666, 1083
Reindl, B., Tammann, G. A., Sandage, A., & Saha, A. 2005, ApJ, 624, 532
Riess, A. G., Press, W. H., & Kirshner, R. P. 1996, ApJ, 473, 588
Riess, A. G., Filippenko, A. V., Challis, P., et al. 1998, AJ, 116, 1009
Sako, M., Bassett, B., Becker, A., et al. 2008, AJ, 135, 348
Salvo, M. E., Cappellaro, E., Mazzali, P. A., et al. 2001, MNRAS, 321, 254
Sauer, D. N., Mazzali, P. A., Blondin, S., et al. 2008, MNRAS, 391, 1605
Scalzo, R. A., Aldering, G., Antilogus, P., et al. 2010, ApJ, 713, 1073
Sollerman, J., Mörtsell, E., Davis, T. M., et al. 2009, ApJ, 703, 1374
Spyromilio, J., Gilmozzi, R., Sollerman, J., et al. 2004, A&A, 426, 547
Stanishev, V., Goobar, A., Benetti, S., et al. 2007, A&A, 469, 645
Sullivan, M., Le Borgne, D., Pritchet, C. J., et al. 2006, ApJ, 648, 868
Sullivan, M., Ellis, R. S., Howell, D. A., et al. 2009, ApJ, 693, L76
Sullivan, M., Conley, A., Howell, D. A., et al. 2010, MNRAS, 406, 782
Taubenberger, S., Hachinger, S., Pignata, G., et al. 2008, MNRAS, 385, 75
Tripp, R. 1998, A&A, 331, 815
Turatto, M., Benetti, S., Cappellaro, E., et al. 1996, MNRAS, 283, 1
Turatto, M., Piemonte, A., Benetti, S., et al. 1998, AJ, 116, 2431
Valentini, G., Di Carlo, E., Massi, F., et al. 2003, ApJ, 595, 779
Vanden Berk, D. E., Richards, G. T., Bauer, A., et al. 2001, AJ, 122, 549
Vinkó, J., Bíró, I. B., Csák, B., et al. 2003, A&A, 397, 115
Wang, L., Baade, D., Höflich, P., et al. 2003, ApJ, 591, 1110
Wang, X., Filippenko, A. V., Ganeshalingam, M., et al. 2009, ApJ, 699, L139
Wood-Vasey, W. M., Miknaitis, G., Stubbs, C. W., et al. 2007, ApJ, 666, 694
Yamanaka, M., Naito, H., Kinugasa, K., et al. 2009, PASJ, 61, 713
Yip, C. W., Connolly, A. J., Szalay, A. S., et al. 2004, AJ, 128, 585
York, D. G., Adelman, J., Anderson, Jr., J. E., et al. 2000, AJ, 120, 1579
Zheng, C., Romani, R. W., Sako, M., et al. 2008, AJ, 135, 1766

Pages 23 to 31 are available in the electronic edition of the journal at http://www.aanda.org

Appendix A: Host-galaxy subtraction uncertainties and evolution detection limits

Estimation of the SED of contaminating host galaxy light is an essential step if spectral indicators in contaminated and uncontaminated spectra are to be compared. This will, in turn, be unavoidable when comparing nearby (usually with the SN clearly separated from the host galaxy core) and distant SNe (where SN and galaxy light are degenerate). In Östman et al. (2010) we present the host-galaxy subtraction pipeline applied to the NTT/NOT SNe. In short this method consists in matching a SN template with a number of galaxy eigencomponent spectra, including a slit loss/reddening correction. Even if the observed SN SED deviates slightly from the SN templates used in the fit, the very large number of wavelength bins compared with the few fit parameters (five) will allow this SN deviations to remain after the subtraction.

However, the host subtraction produces an increased indicator measurement uncertainty and possibly a bias. It is important that this uncertainty or bias is estimated. In this Appendix we describe the extensive simulations that were run to study the effectiveness of the host subtraction. These simulations were used to calculate a systematic bias and uncertainty for every measurement, depending on the shape of the indicator and contamination level.

As a second step of these simulations we used suggested (metallicity) evolution models to study under which circumstances these would be detected assuming the properties of the NTT/NOT data set.

A.1. The subtraction pipeline

The subtraction pipeline is described in detail in Östman et al. (2010). The input parameters are flux density and (optionally) error, observer frame wavelength, redshift and an epoch estimate. This pipeline thus operates identically for real and simulated spectra. A range of internal fit parameters can be changed, including which templates and host galaxy eigencomponent spectra are used as well as the nature of slit loss/extinction approximation. The fit parameters were optimised and fixed during a series of test runs.

A.2. Synthetic spectrum simulations

To test the reliability of the estimated host galaxy spectra and the impact on spectral indicators, a large number of simulated contaminated spectra were created. Besides contamination, these simulations included realistic slit loss and noise levels. The synthetic spectra are created from

- *A supernova spectrum*. The SN spectra used as templates all have high S/N and low contamination. Their epochs are similar to the ones of the NTT/NOT spectra[9]. Eleven different SN spectra are used: five of SN 2003du (epochs −6, −2, 4, 9, 10, 17) (Stanishev et al. 2007), one of SN 1998aq (Branch et al. 2003) at peak brightness, two of the subluminous SN 1999by (epochs −5 and 3) (Garnavich et al. 2004) and two of the peculiar and luminous SN 1999aa (epochs −5 and 0) (Garavini et al. 2004).
- *Reddening is added to the SN spectrum*. The reddening is added using the Cardelli et al. (1989) extinction law using a total-to-selective extinction ratio R_V of 2.1 and a colour excess $E(B-V)$ drawn from the distribution of $E(B-V)$ obtained from the NTT/NOT lightcurve fits.
- *A galaxy spectrum*. Four galaxy templates of varying type (elliptical, S0, Sa and Sb) from Kinney et al. (1996) are used together with three real galaxy spectra observed at NTT at the same time as the SN spectra analysed here (host galaxy spectra for SDSS SN7527, SN13840 and SN15381). The contamination level is randomly chosen between 0 and 70% for the g band. These simulations were later extended in a second series where 50 randomly chosen SDSS galaxy spectra were used. Figures displayed here are based on the first run series, but results are similar when including the second set of galaxy spectra.
- *Redshift*. The object redshift is randomly drawn from the NTT/NOT redshift distribution.
- *Slit loss is added to the SN spectrum*. The differential slit loss functions are taken from Östman et al. (2010) and correspond to typical NTT/NOT situations and range from insignificant to severe.
- *Noise addition*. A S/N value is randomly chosen from the NTT/NOT spectral S/N distribution. Poisson noise is added to the spectra until the target S/N is achieved. The shape of the noise is determined as a linear combination of the input spectrum and a randomly chosen NTT/NOT sky spectrum. The linear combination is regulated such that the highest S/N value in the NTT/NOT sample corresponds to no contribution from sky noise, the lowest S/N corresponds to complete dominance by sky noise and intermediate values to a combination of the two error sources.

All of the created synthetic spectra were then processed through the host subtraction pipeline and spectral indicators were measured. The measured spectral indicators could then be compared with the ones obtained from the original SN spectrum. The subtractions were thus evaluated only with respect to how well correct indicators were measured.

A.3. Simulation results

The simulation results can be analysed in a number of ways: Looking at specific SN spectra, specific galaxy types, spectra with more or less slit loss or contamination or any combination of these. For each of these subgroups errors in all equivalent widths and velocities can be calculated.

In general simulations are stable with the following characteristics: a small bias for very low contamination levels that decrease with added contamination and a random dispersion that increases with contamination. The size of these effects vary slightly from feature to feature. The small bias for low level contamination means that the subtraction pipeline finds "something" to subtract even when no contamination was added. This is fully consistent with having a small amount of host light *already present* in the template spectra. But we cannot rule out that that a part of this bias is caused by the subtraction methods. In practise we do not perform host subtraction on spectra with very low contamination levels. In all cases the full bias as estimated in the simulations is retained, thus generally overestimating the bias levels.

Sample simulation results are presented in Fig. A.1.

The simulations were evaluated with and without added noise. Noise was found to increase the error dispersion but not introduce any significant bias. The added dispersion was comparable to uncertainties yielded from the designated noise

[9] These templates are omitted from the subtraction pipeline since this would make the fit trivial.

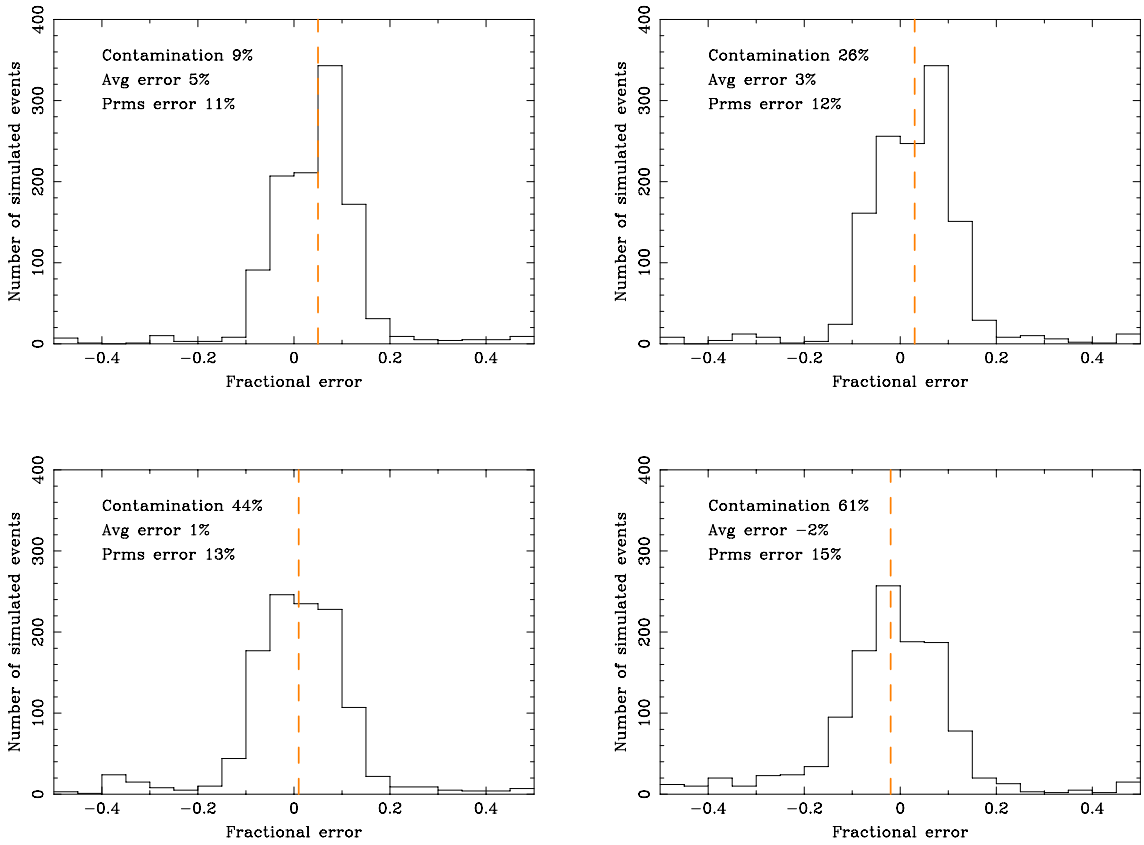

Fig. A.1. Sample host contamination simulations results. For every simulated spectrum the final fractional error is calculated (fractional error is used so that all templates of different epoch and subtypes can be added and analysed as function of contamination). The panels show the distribution of errors, divided into four contamination bins (0−17.5, 17.5−35, 35−52.5 and 52.5−70% in *g* band). The average contamination, average error and Population RMS (Prms) is printed for each bin. The average error (shown as dashed orange line) indicates a small bias, *decreasing* with contamination. The dispersion indicates a random error from host subtraction, increasing with contamination. These plots are based on pEW f3; other pEWs show similar results.

simulations. We thus separate errors from host contamination and noise. See Appendix B for a further discussion about noise and filtering. For final spectra the systematic uncertainties will be the sum in quadrature of the respective subtraction and noise systematic uncertainties.

A.4. Alternative subtraction methods

A number of alternative host subtraction methods were tried. These included two fundamentally different fitting methods: linear fits using all nearby SN spectra as SN templates and photometry fixed galaxy subtraction where the host galaxy photometry is used to constrain the galaxy shape and proportion. Both methods relax the dependence on the SN template, the first through including a larger variety of such and the second through not using any template at all. However, in general the multiplicative method including the slit loss/reddening correction was found to be superior in most cases and generally more stable.

A number of different implementations of the subtraction pipeline were also tried. These included modifying the number of galaxy eigenspectra, the origin of these eigenspectra and changing constraints on the eigenspectra proportions. The host galaxy subtraction method described above was the final product of these tests.

However, there will be individual objects, for which the host subtraction fails or performs less than ideal. This is a natural consequence of the degeneracy between SN, host galaxy and noise. For some of these objects alternative subtraction methods could have been better suited, but for consistency uniform host subtractions were used. The simulations were designed to estimate the bias caused by such failed subtractions.

A.5. Evolution models

Since it is unknown if evolution exists and how it, if existing, affects the SN Ia SED, it is impossible to predict whether evolution could be detected with the NTT/NOT SNe. But we can still study proposed models to quantify how well these effects would be detected. Two different models were considered here: first ad hoc decrease of the depth of feature 3 and 4, where the *frac* parameter regulates the percent decrease of these depths. This modification was inspired by the indication of changes in these features seen by Foley et al. (2008) and Sullivan et al. (2009). As a second set of models we use the spectral changes caused by one low and one high metallicity model simulated by Lentz et al. (2000). For spectrum templates with epochs less than −2.5 the 15 days after explosion model was used, otherwise the day +20 model.

All base SN templates used in the above simulations were modified according to the evolution models, and processed through the subtraction and measurement pipelines again. The modifications as applied to the SN spectrum of SN2003du observed at April 30 2003 is displayed in Fig. A.2.

These models should not be considered realistic evolutionary models to be tested, but rather tests as to what level of

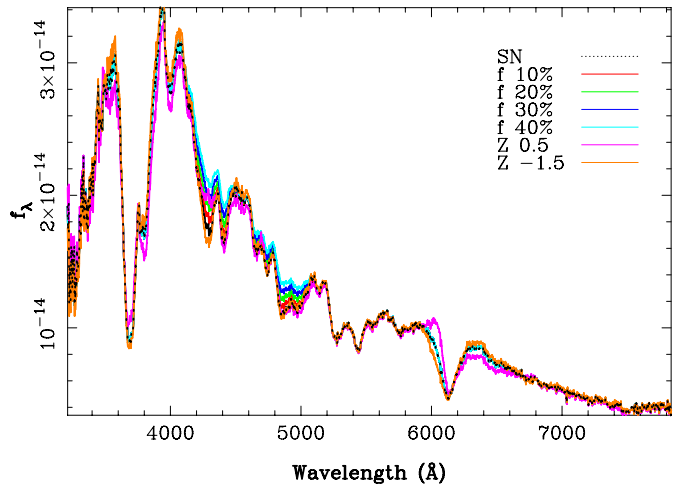

Fig. A.2. Models of evolution/metallicity changes applied to SN2003du. f (frac) models consist of a decrease in the depth of the f3 and f4 features, Z 0.5 corresponds to the Lentz et al. (2000) model of increased metallicity, Z −1.5 corresponds to the Lentz et al. (2000) model of decreased metallicity.

evolution can be detected assuming host subtraction uncertainties. They are however, examples of evolution that would not be detected by visual inspection of noisy data but could still effect SN Ia cosmology.

A.6. Evolution detection limits

All measurements on "evolved" host galaxy subtracted spectra are collected and compared to the true unevolved reference values. This difference between measurements can then be compared with the estimated statistical and systematic uncertainties and the likelihood of detecting the evolution studied. Sample evolution detection probabilities for evolved SNe is shown in Fig. A.3.

These comparisons show that most evolved SNe would be detected. However, the detection limits we are searching for must be realistic: we do not expect all SNe at higher redshift to be evolved, but rather the fraction of e.g. low metallicity SNe will change. To study this limit we designed a further simulation based on the NTT/NOT redshift distribution. The probability of each SN to be evolved according to one of the above models, is set to be proportional to redshift and reach 50% at the average redshift of the NTT/NOT data set. For each model we repeat the measurement 5000 times and in each we randomly select which SNe are evolved. The total spectral indicator offset is calculated and compared to the uncertainties, thus obtaining a distribution of the evolution detection limit.

In Table A.1 detection limits assuming all NTT/NOT SNe (*including high contamination*) are listed for a number of indicators for the models for evolution/metallicity discussed above. These limits are completely dominated by the systematic bias levels of the high contamination events, since the systematic bias is set to be a systematic floor where the largest bias contained is used. A more realistic and less conservative estimate arises when we remove the highest bias/contamination events; these limits are given in Table A.2.

These results show that we would be sensitive to all but the very weakest of these evolution models using at least one indicator, albeit at a fairly low significance level.

Table A.1. Probability of detecting models for SN Ia evolution.

Indicator	0	10	20	30	40	Low-met	Hi-met
pEW f3	0	0	1	1	1	1	0
pEW f4	0	0	1	1	1	0	0
Vel f3	0	0	0	0	0	0	0
Vel f7	0	0	0	0	0	2	0
pEW f3+f4	0	0	1	*	2	1	1

Notes. Each column corresponds to one model (first column is no evolution), see text for further description. Each row corresponds to a search for evolution using the specified spectral indicator, assuming the population changes linearly with redshift. Numbers are the detection level in standard deviations *using max statistical/systematic error as irreducible global error*. The last line is an example where measurements of two indicators are combined to increase sensitivity ("*" = comparison not made).

Table A.2. Probability of detecting models for SN Ia evolution.

Indicator	0	10	20	30	40	Low-met	Hi-met
pEW f3	0	1	2	3	5	3	2
pEW f4	0	1	2	3	4	0	1
Vel f3	0	0	0	1	2	1	2
Vel f7	0	0	0	0	0	4	1
pEW f3+f4	0	1	3	4	5	2	2

Notes. Each column corresponds to one model (first column is no evolution), see text for further description. Each row corresponds to a search for evolution using the specified spectral indicator, assuming the population changes linearly with redshift. Numbers are the detection level in standard deviations *when removing highest bias events*. The last line is an example where measurements of two indicators are combined to increase sensitivity.

A.7. Velocity host subtraction errors

Host contamination could affect velocity measurements either through introducing a false minimum or through modifying the position of the true minimum. Studies of simulated spectra show that velocity errors do increase with contamination, but below an *r*-band contamination of 60%, the errors are small compared to statistical and noise uncertainties.

Host subtraction methods in general perform similarly. The same subtractions as for pEWs are used (for consistency). Systematic uncertainties as estimated from the simulations are added to all measurements.

Appendix B: Filtering and uncertainties due to noise

Random noise will degrade data quality, making measurements less accurate. For low S/N SN spectra, the conventional solution is to apply a filter to remove the high-frequency noise. This technique works well if small levels of filtering are used (filtering/smoothing are considered identical processes here), where the true shape is clearly visible. For noisy data it is no longer obvious what filter to use or how accurate results are.

According to the definition, pseudo-equivalent widths run from one wavelength extremum point to another. This makes such measurements extremely sensitive to noise: if any noise peaks remain, the pseudo continuum will be defined from there. To remove these, and create unbiased data, strong filtering is needed for low S/N data. We would, however, not want to filter high S/N spectra (at any redshift) too much since this

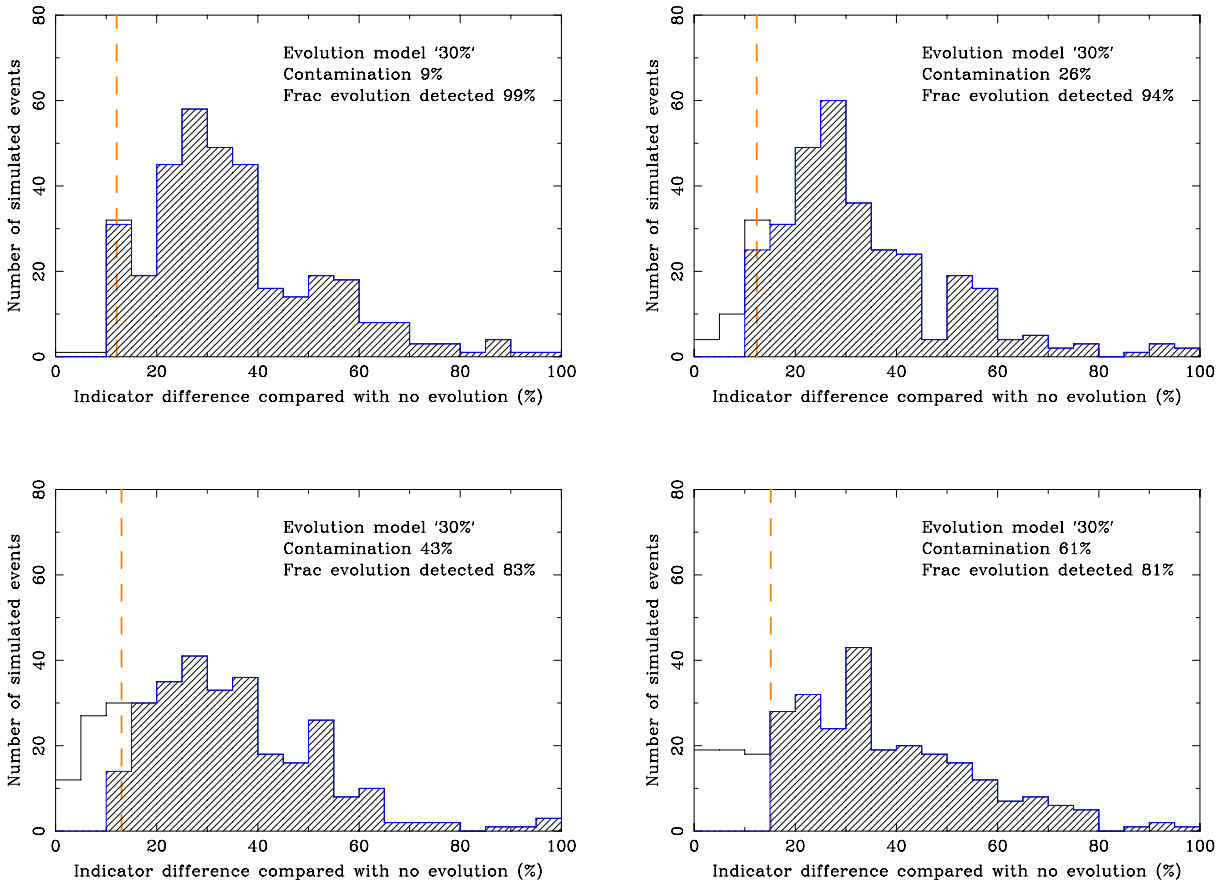

Fig. A.3. Sample study of how well evolution is detected in simulated spectra. The "30%" evolution model was applied to all template spectra and the measured indicators compared with the unevolved measurements. The panels show the distribution of fractional difference, divided into the same contamination bins as in Fig. A.1. The total uncertainty in each bin (bias and dispersion) as estimated above is shown as an orange dashed line. *Events where the reported difference is larger than uncertainties would be seen as deviating*. In this sense detectable events are shown as hashed bins. The fraction of detected events is shown in each panel. This fraction decreases with contamination.

would destroy information. We would also like to estimate noise uncertainties.

A further complication caused by filtering is that errors in filtered bins are correlated.

A series of Monte Carlo simulations were run in order to (i) compare filter methods; (ii) determine filter parameters and (iii) estimate associated uncertainties (while avoiding having to determine filtered error correlations). These simulations are described below.

B.1. Filter method comparison

Three filters easy to implement are (1) the boxcar filter, which is simple averaging over a wavelength range, (2) the variance-weighted Gaussian filter where the smoothed value in a pixel is determined from a surrounding region weighted by a Gaussian determined by the inverse variance[10] and (3) the FFT filter, where all frequencies above a certain maximum frequency are removed from the spectrum.

In order to determine which filter method works best and find optimal filter parameters, MC simulations were run. Random noise was added to template SN spectra after which the S/N was determined, the spectra filtered and indicators measured. For each method the optimal filter parameters were found through minimisation vs. the true value. This process was repeated until MC errors were sufficiently small. It was found that there is no optimal method with a single set of parameters that worked over the complete range of varying features and S/N values. All methods *can* yield non-biased values if correct filter parameters are used. The correct filter parameters should be determined by the actual noise level and the nature of the feature studied (broad or sharp).

Since all methods can be made to work but none will work with a single set of parameters, we selected the simplest method, the boxcar filter, as described below.

B.2. Optimal boxcar filter parameters for pEW measurements

The above simulations showed that true pseudo-equivalent widths can be measured from noisy spectra after binning, but correct bin widths must be used. A range of MC simulations were run to determine the widths to use and the typical errors caused by noise. This procedure is detailed below.

Noise was generated with a certain amplitude. A gradually stronger filter was applied, while measuring relevant features at each stage. Through comparison with the true, noiseless values, the errors are obtained. For each iteration a "pseudo-S/N" is calculated as follows: a minimal boxcar (spanning three bins) is applied, and a pseudo-S/N can be calculated by comparing this with the original spectrum. This value serves as an initial estimation of noise level, and can later be compared to real spectra (adjusting for bin widths). A pseudo-S/N is feature relative,

[10] See Blondin et al. (2006) for a more detailed description.

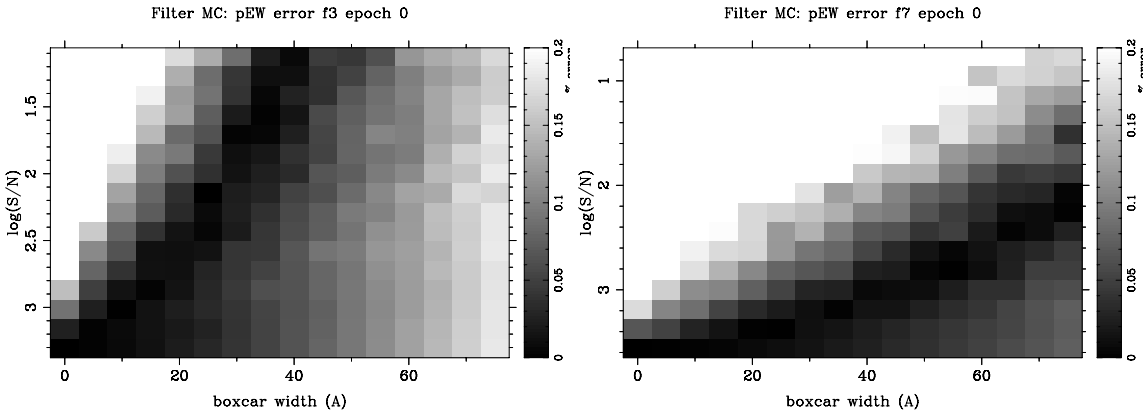

Fig. B.1. Average pEW error for feature 3 (*left panel*) and feature 7 (*right panel*) at the epoch of maximum light. The noise level, expressed through the logarithm of the pseudo-S/N, increases along the *y*-axis and the filter strength along the *x*-axis. Darker shades show smaller errors.

and calculated within the maximum boundaries of the feature in question.

This procedure is repeated 100 times for each noise amplitude[11]. For each filter strength and pseudo-S/N we thus have a range of pEW errors, from which we obtain the average and dispersion. Two sample mappings of these errors are displayed in Fig. B.1 (for these maps we have used *absolute* errors). It is seen that for any pseudo-S/N it is possible to define filter strengths yielding small errors (dark shades in figure), *but* the optimal filter strength varies with pseudo-S/N.

These maps are used to find the correct filter for a given feature and pseudo-S/N. Separate maps are created for each feature, where broad features typically demand stronger filtering. Furthermore, the *dispersion* of pEW-values in the optimal bin can be used to approximate the systematic error of doing pEW measurements on noisy spectra[12].

Note that it is the shape of the feature that determines correct filtering, and that this evolves with epoch. To correctly account for this, the above procedure was repeated for each epoch of the Hsiao templates (Hsiao et al. 2007). The templates were interpolated to 2.5 Å bins in all simulations.

Simulation results are written to a table. These provide, for every feature and lightcurve epoch, the best filter-width to use to minimise the risk for noise bias. Since only the pseudo-S/N is used, we do not require error spectra.

The application to real data can be summarised as:

1. A minimal boxcar is applied, through which the pseudo-S/N is determined.
2. By comparing Monte-Carlo runs for the Hsiao template of the same epoch and feature, the optimal boxcar width is determined.
3. The average MC error and dispersion around the reference values are taken as systematic errors from the simulation.

B.3. Velocity noise errors

For the well-defined type Ia SN minima studied here, minimum positions are stable relative to noise as long as sufficiently wide bins are used. A constant bin width in velocity space can thus be used. However, determinations of minima will still be affected by noise to the degree that on average noisy data will have larger dispersion. Both these effects, that no bias occurs and the increased dispersion, were studied using MC simulations of the Hsiao templates using the same approach as for pEWs. Random noise is added to the Hsiao templates (Hsiao et al. 2007) and the velocities are calculated after binning.

For every template epoch and feature, both bias and dispersion are obtained as functions of pseudo-S/N. For velocities 2, 3, 5, 6 and 7 (and reasonable epoch intervals), these results are consistent with no bias and a gradual increase in dispersion with noise.

For each spectrum studied (in both the reference and NTT/NOT set), epoch and pseudo-S/N values were used to locate the corresponding MC dispersion, which was used as systematic velocity error.

For features with more complicated minima (feature 4) or possible additional high velocity absorption features (feature 1), simply determining the minima will not be enough. These features demand either stringent minima criteria or function fitting for optimal study. Automatic minima measurements will show a large scatter.

[11] Repeated tests were run to verify that results were not sensitive to the number of iterations.

[12] This systematic error would only include pure noise effects and not e.g. effects like host galaxy contamination.

Appendix C: Data tables

Table C.1. Supernova spectra.

SN	epochs (days)	Spec source	LC source
SN1983g	6, 7	Cristiani et al. (1992)	–
SN1986g	–4, –4, –4, –3, –3, –2, –1, 0, 1, 21	Hamuy et al. (2002)	Arsenijevic et al. (2008)
SN1989b	0, 6, 11, 21, 22	Barbon et al. (1990)	Arsenijevic et al. (2008)
SN1990n	2	Mazzali et al. (1993); Gómez & López (1998)	Arsenijevic et al. (2008)
SN1991bg	1, 1, 2, 2, 16, 18, 20, 29	Turatto et al. (1996); Gomez et al. (1996)	Arsenijevic et al. (2008)
SN1991m	3, 28	Gómez & López (1998)	Arsenijevic et al. (2008)
SN1991s	14	Gómez & López (1998)	–
SN1991t	–12, –11, –10, –9, –8, –7, –6	Mazzali et al. (1995); Gómez & López (1998)	Arsenijevic et al. (2008)
SN1992g	15	Gómez & López (1998)	–
SN1994d	–11, –11, –10, –9, –8, –5, –4, –2, 2, 2, 3, 4, 4, 5, 7, 10, 10, 11, 11, 12, 13, 15, 17, 19, 24, 26	Patat et al. (1996); Gómez & López (1998)	Arsenijevic et al. (2008)
SN1994q	10	Gomez et al. (1996)	–
SN1994s	22	Gomez et al. (1996)	Hicken et al. (2009)
SN1996x	–4, –2, –1, 0, 1, 3, 7, 12, 22, 24	Salvo et al. (2001)	Kowalski et al. (2008)
SN1997br	–9, –8, –7, –6, –4, 8, 24	Li et al. (1999)	Arsenijevic et al. (2008)
SN1997cn	3, 28	Turatto et al. (1998)	Arsenijevic et al. (2008)
SN1997do	–12, –11, –8, –7, 8, 10, 11, 12, 14, 15, 20, 21	Matheson et al. (2008)	Kowalski et al. (2008)
SN1997dt	–11, –10, –9, –8, –5, 0, 2	Matheson et al. (2008)	Kowalski et al. (2008)
SN1998ab	–8, 17, 18, 19, 20, 21, 22	Matheson et al. (2008)	Hicken et al. (2009)
SN1998aq	–9, –8, –3, 0, 0, 1, 1, 2, 2, 3, 3, 4, 4, 5, 5, 6, 6, 7, 18, 19, 20, 21, 23, 24, 30	Matheson et al. (2008); Branch et al. (2003)	Arsenijevic et al. (2008)
SN1998bu	–4, –4, –3, –3, –2, –2, 0, 8, 8, 9, 9, 10, 10, 10, 11, 11, 12, 12, 13, 13, 27, 27, 28, 28, 29, 29, 30	Matheson et al. (2008); Jha et al. (1999); Cappellaro et al. (2001); Spyromilio et al. (2004)	Arsenijevic et al. (2008)
SN1998dh	–9, –9, –8, –6, –4, –1	Matheson et al. (2008)	Kowalski et al. (2008)
SN1998dm	4, 5, 7, 10, 12, 15, 17, 24	Matheson et al. (2008)	
SN1998eg	–1, 4, 5, 17, 19, 23	Matheson et al. (2008)	Hicken et al. (2009)
SN1998v	0, 1, 2, 11, 12, 14	Matheson et al. (2008)	Hicken et al. (2009)
SN1999aa	–11, –11, –10, –9, –8, –7, –7, –7, –6, –5, –4, –3, –3, –3, –2, –1, –1, 0, 5, 5, 6, 6, 14, 14, 14, 15, 16, 17, 19, 19, 25, 25, 27, 28, 28, 28, 29, 30	Matheson et al. (2008); Garavini et al. (2004, 2007a)	Hicken et al. (2009)
SN1999ac	–15, –15, –11, –9, –9, –3, 0, 0, 2, 2, 2, 7, 8, 8, 11, 11, 16, 16, 24, 28, 28	Matheson et al. (2008); Garavini et al. (2005); Phillips et al. (2006); Garavini et al. (2007a)	Kowalski et al. (2008)
SN1999af	–5, 1, 15, 17, 17, 25	Garavini et al. (2007a)	–
SN1999ao	5, 7, 9, 12, 17	Garavini et al. (2007a)	Hicken et al. (2009)
SN1999ar	5	Garavini et al. (2007a)	Hicken et al. (2009)
SN1999au	11, 15, 18, 21	Garavini et al. (2007a)	–
SN1999av	2, 5, 9, 30	Garavini et al. (2007a)	–
SN1999aw	3, 5, 9, 12, 15, 23, 30	Garavini et al. (2007a)	Hicken et al. (2009)
SN1999be	14, 19, 26	Garavini et al. (2007a)	–
SN1999bi	5, 11, 12, 26	Garavini et al. (2007a)	Hicken et al. (2009)
SN1999bk	4, 6, 8	Garavini et al. (2007a)	–
SN1999bm	3, 5, 24	Garavini et al. (2007a)	Hicken et al. (2009)
SN1999bn	2, 12, 19, 24	Garavini et al. (2007a)	Hicken et al. (2009)
SN1999bp	–2, 0, 1, 6, 16, 21	Garavini et al. (2007a)	Hicken et al. (2009)
SN1999bq	3, 3, 16, 20, 24	Garavini et al. (2007a)	–
SN1999by	–5, –5, –4, –4, –3, –3, –2, –2, 1, 2, 3, 3, 3, 4, 4, 5, 5, 6, 6, 6, 7, 7, 8, 9, 10, 11, 16, 24, 25, 28, 29	Matheson et al. (2008); Garnavich et al. (2004); Garavini et al. (2007a)	Arsenijevic et al. (2008)
SN1999cc	–4, –2, –1, 1, 18, 23, 25	Matheson et al. (2008)	Hicken et al. (2009)
SN1999ee	–11, –9, –4, –2, 0, 5, 7, 9, 14, 17, 20, 25, 30	Hamuy et al. (2002)	Arsenijevic et al. (2008)
SN1999ej	–1, 2, 4, 8, 11	Matheson et al. (2008)	Kowalski et al. (2008)

Table C.1. continued.

SN	epochs (days)	Spec source	LC source
SN1999gd	2, 9, 27	Matheson et al. (2008)	Hicken et al. (2009)
SN1999gp	–5, –2, 0, 3, 5, 7, 22	Matheson et al. (2008)	Hicken et al. (2009)
SN2000cf	3, 4, 14, 16, 24, 25	Matheson et al. (2008)	Hicken et al. (2009)
SN2000cn	–10, –9, –8, 8, 10, 12, 21, 26, 27	Matheson et al. (2008)	Hicken et al. (2009)
SN2000cx	–4, –3, –2, –1, 0, 1, 5, 6, 7, 9, 11, 14, 19, 22, 24, 26, 28, 30	Matheson et al. (2008); Li et al. (2001)	Arsenijevic et al. (2008)
SN2000dk	–5, –4, 1, 4, 9	Matheson et al. (2008)	Hicken et al. (2009)
SN2000e	–9, –6, –5, 5	Valentini et al. (2003)	Arsenijevic et al. (2008)
SN2000fa	–11, –11, 1, 2, 4, 9, 11, 14, 16, 18, 20	Matheson et al. (2008)	Hicken et al. (2009)
SN2001el	9, 14, 22	Wang et al. (2003)	Krisciunas et al. (2003)
SN2001v	–14, –13, –12, –11, –10, –8, –7, –6, –4, 9, 10, 11, 12, 13, 18, 19, 20, 20, 21, 21, 22, 23, 24, 27, 28	Matheson et al. (2008,?)	Vinkó et al. (2003)
SN2002bo	–14, –13, –11, –6, –5, –5, –4, –3, –3, –2, –1, 4, 28	Benetti et al. (2004)	Arsenijevic et al. (2008)
SN2002dj	–11, –10, –9, –8, –6, –4, –3, 9, 10, 13, 17, 22	Pignata et al. (2008)	Hicken et al. (2009)
SN2002er	–11, –9, –8, –7, –6, –5, –4, –3, –2, –1, 0, 2, 4, 5, 6, 10, 12, 13, 16, 17, 20, 25	Kotak et al. (2005)	Arsenijevic et al. (2008)
SN2003cg	–9, –8, –7, –5, –2, –2, –1, 1, 4, 7, 10, 11, 12, 16, 19, 23, 23, 26, 28	Elias-Rosa et al. (2006)	Arsenijevic et al. (2008)
SN2003du	–13, –11, –11, –11, –8, –7, –6, –5, –4, –3, –2, –1, 0, 0, 1, 2, 2, 3, 4, 6, 6, 7, 8, 9, 9, 10, 13, 15, 17, 18, 19, 21, 24, 26	Stanishev et al. (2007); Anupama et al. (2005); Gerardy (2005)	Arsenijevic et al. (2008)
SN2004dt	–10, –9, –9, –7, –7, –6, –6, –4, –4, –3, –2, –1, –1, 2, 3, 4, 14, 17, 21	Altavilla et al. (2007)	–
SN2004eo	–11, –6, –3, 2, 7, 11, 13, 14, 21, 22, 24, 30	Pastorello et al. (2007)	Arsenijevic et al. (2008)
SN2004s	1, 7, 12, 13, 13, 18	Krisciunas et al. (2007)	Arsenijevic et al. (2008)
SN2005bl	–6, –5, –3, –3, 4, 12, 19, 21	Taubenberger et al. (2008)	–
SN2005cf	–12, –12, –11, –10, –10, –9, –7, –7, –6, –4, –3, –1, 0, 4, 4, 5, 6, 7, 9, 12, 12, 14, 16, 25, 29	Garavini et al. (2007b); Leonard (2007)	Arsenijevic et al. (2008)
SN2005cg	–10, –9, –4, 0, 5, 7	Quimby et al. (2006)	–
SN2005hj	–6, 0, 2, 5	Quimby et al. (2007)	Hicken et al. (2009)
SN2005hk	–8, –7, –6, –6, –5, –4, –4, –3, 4, 13, 15, 24, 27	Phillips et al. (2007)	Arsenijevic et al. (2008)
SN2006gz	–14, –14, –13, –13, –12, –10, –9, –5, –2, 5, 6, 7, 8, 8, 9, 10, 11	Hicken et al. (2007)	Arsenijevic et al. (2008)
SN2006x	–10, –7, 0	Yamanaka et al. (2009)	–

Table C.2. NTT/NOT spectra.

ID	IAU	SPID	Epochs (days)
12781	2006er	680	10.9
12843	2006fa	727	10.2
12853	2006ey	685	10.3
12856	2006fl	695	–3.2
12860	2006fc	688	–1.9
12898	2006fw	712	–6.6
12930	2006ex	687	10.1
12950	2006fy	700	–4.4
13025	2006fx	761	3.4
13044	2006fm	724, 1062	–8.2, 20.2
13070	2006fu	736	6.9
13072	2006fi	723	0.0
13135	2006fz	739, 998	–7.7, 17.6
13796	2006hl	1058, 1058	12.7, 12.7
13894	2006jh	1039	9.2
14157	2006kj	1040	9.4
14437	2006hy	1061	14.0
14846	2006jn	1014	–1.7
14871	2006jq	1008	–4.2
14979	2006jr	1009	–2.1
14984	2006js	1027	–1.2
15129	2006kq	1015	1.8
15132	2006jt	1012	–2.4
15161	2006jw	1010	–1.0
15171	2006kb	1045, 1045	–5.7, –5.7
15203	2006jy	1026	–2.4
15222	2006jz	1004	–5.8
15259	2006kc	1051	–1.9
16021	2006nc	1355	11.3
16069	2006nd	1467	11.5
16165	2006nw	1326	2.6
16215	2006ne	1456	4.3
16287	2006np	1449, 1449, 1569, 1569, 1650	2.4, 2.4, 3.3, 3.3, 19.5
16352	2006pk	1478	4.1
16473	2006pl	1520	1.3
16637		1514	–0.9
17332	2007jk	1899	3.3
17366	2007hz	1782	8.9
17389	2007ih	1811	7.0
17435	2007ka	1902, 1902	2.7, 2.7
17497	2007jt	1837	–2.4
17552	2007jl	1789	3.5
17745	2007ju	2161	15.1
17784	2007jg	1842	–5.5
17790	2007jx	1887	1.0
17811	2007ix	1816, 1816	4.6, 4.6
17825	2007je	1819	–4.9
17875	2007jz	1817	0.3
17880	2007jd	1843, 1957	–1.9, 1.2
17886	2007jh	1844	–4.5
18325	2007mv	2277	8.6
18466	2007lm	2270	4.5
18768	2007lh	2135	6.7
18787	2007mf	2150	0.2
18804	2007me	2148	–5.0
19023	2007ls	2236	–1.7
19101	2007ml	2268, 2268	–6.0, –6.0
19149	2007ni	2275, 2275	–7.1, –7.1
19155	2007mn	2607	18.7
19282	2007mk	2280	–8.2
19341	2007nf	2298	–2.4
19353	2007nj	2281	–7.3
19381	2007nk	2283, 2283	–3.5, –3.5
19899	2007pu	2550	1.2
19913	2007qf	2585	9.6

Table C.2. continued.

ID	IAU SPID	Epochs (days)	
19953	2007pf	2602	4.2
19968	2007ol	2549	5.2
20039	2007qh	2584	7.6
20040	2007rf	2612	6.4
20142	2007qg	2586	4.7
20144	2007ql	2541	1.1
20345	2007qp	2567, 2567	–0.7, –0.7
20364	2007qo	2581	–1.3
20430	2007qj	2543	1.4
20625	2007px	2551, 2604	–5.4, –3.6
21006	2007qs	2566	1.7
21033	2007qy	2565	–3.3
21034	2007qa	2719	13.3
21042	2007qz	2564	–6.4
21422	2007rq	2599	–3.6
21502	2007ra	2574, 2575	–8.6, –7.7